

¹ **GLO-Roots: an imaging platform enabling multidimensional characterization of soil-grown roots systems**

³ Rubén Rellán-Álvarez^{1, 9}, Guillaume Lobet², Heike Lindner^{1, 8}, Pierre-Luc Pradier^{1, 8, 10},
⁴ Jose Sebastian^{1, 8}, Muh-Ching Yee¹, Yu Geng^{1, 7}, Charlotte Trontin¹, Therese LaRue³,
⁵ Amanda Schrager-Lavelle⁴, Cara H. Haney⁵, Rita Nieu⁶, Julin Maloof⁴, John P. Vogel⁷,
⁶ José R. Dinneny^{1, 12}

⁷ ¹ Department of Plant Biology, Carnegie Institution for Science, Stanford, CA, USA.

⁸ ² PhytoSystems, University of Liège, Liège, Belgium.

⁹ ³ Department of Biology, Stanford University, Stanford, CA, USA.

¹⁰ ⁴ Department of Plant Biology, UC Davis, Davis, CA, USA.

¹¹ ⁵ Harvard Medical School/Massachusetts General Hospital, Department of Genetics/¹² Department of Molecular Biology Boston, MA, USA

¹³ ⁶ USDA Western Regional Research Center, Albany, CA, USA

¹⁴ ⁷ DOE Joint Genome Institute, Walnut Creek, CA, USA

¹⁵ ⁸ These authors contributed equally

¹⁶ ⁹ Present address: Laboratorio Nacional de Genómica para la Biodiversidad (Langebio),
¹⁷ Unidad de Genómica Avanzada, Centro de Investigación y de Estudios Avanzados del Insti-
¹⁸ tuto Politécnico Nacional (CINVESTAV-IPN), Irapuato, Guanajuato, México

¹⁹ ¹⁰ Present address: Boyce Thompson Institute for Plant Research/USDA, Ithaca, NY, USA.

²⁰ ¹¹ Present address: Energy Biosciences Institute, UC, Berkeley, CA, USA

²¹ ¹² Corresponding author

²² **Author contributions:**

²³ RR-A: Conception, design and development of the growth and imaging system and Arabidop-
²⁴ sis transgenic lines; acquisition, analysis and interpretation of data; drafting and revising

25 the article.

26 GL: Development of the GLO-RIA image analysis plugin, analysis and interpretation of

27 data, drafting and revising the article.

28 HL: Acquisition of data, development of the tomato growth and imaging setup.

29 P-LP: Acquisition of data, analysis and interpretation of data

30 JS: Development of Brachypodium transgenic lines, acquisition and analysis of Brachy-

31 podium, Arabidopsis and tomato data.

32 MCY: Development of Arabidopsis and Brachypodium transgenic lines.

33 YG: Development of Arabidopsis transgenic lines.

34 CT: Acquisition and analysis of the QPCR data

35 TL: Acquisition and analysis of the QPCR data

36 AS-L: Contributed the unpublished dual-color tomato line.

37 CH: Contributed the unpublished *Pseudomonas fluorescens* CH267-lux strain.

38 RN: Contribution to the development of the Brachypodium transgenic line.

39 JM: Contributed the unpublished dual-color tomato line.

40 JPV: Contribution to the development of the Brachypodium transgenic line.

41 JRD: Conception, design and development of the growth and imaging system and Arabidop-

42 sis transgenic lines; acquisition, analysis and interpretation of data; drafting and revising

43 the article.

44 All authors read and approve the final version of the manuscript.

45 **Abstract**

46 Root systems develop different root types that individually sense cues from their local

47 environment and integrate this information with systemic signals. This complex multi-

48 dimensional amalgam of inputs enables continuous adjustment of root growth rates, direc-
49 tion and metabolic activity that define a dynamic physical network. Current methods for
50 analyzing root biology balance physiological relevance with imaging capability. To bridge
51 this divide, we developed an integrated imaging system called Growth and Luminescence
52 Observatory for Roots (GLO-Roots) that uses luminescence-based reporters to enable stud-
53 ies of root architecture and gene expression patterns in soil-grown, light-shielded roots. We
54 have developed image analysis algorithms that allow the spatial integration of soil prop-
55 erties such as soil moisture with root traits. We propose GLO-Roots as a system that
56 has great utility in presenting environmental stimuli to roots in ways that evoke natural
57 adaptive responses and in providing tools for studying the multi-dimensional nature of such
58 processes.

59 **Introduction**

60 Plant roots are three-dimensional assemblies of cells that coordinately monitor and acclimate
61 to soil environmental change by altering physiological and developmental processes through
62 cell-type and organ-specific regulatory mechanisms^{1,2}. Soil comprises a complex distribution
63 of particles of different size, composition and physical properties, airspaces, variation in
64 nutrient availability and microbial diversity^{3,4}. These physical, chemical and biological
65 properties of soil can vary on spatial scales of meters to microns, and on temporal scales
66 ranging from seasonal change to seconds. Root tips monitor this environment through
67 locally and systemically acting sensory mechanisms^{5,6}.

68 The architecture of the root system determines the volume of soil where resources can be
69 accessed by the plant (rhizosphere) and is under both environmental and genetic control.
70 Plasticity in growth parameters allows the plant to adjust its form to suit a particular soil.
71 Lateral roots, which usually make up the majority of the total root system, often grow at an
72 angle divergent from the gravity vector. This gravity set-point angle (GSA) is controlled by
73 auxin biosynthesis and signaling and can be regulated by developmental age and root type⁷.
74 Recent cloning of the *DRO1* Quantitative Trait Locus (QTL) demonstrates that natural

75 genetic variation is a powerful tool for uncovering such control mechanisms⁸.

76 Specific root ideotypes (idealized phenotypes) have been proposed to be optimal for acquisi-
77 tion of water and nitrogen, which are distinct from ideotypes for low phosphorus. Based on
78 computational modeling and field studies, the “steep, deep and cheap” ideotype proposed by
79 Lynch and colleagues may provide advantages to the plant for capturing water and elements
80 like nitrogen that are water soluble and therefore tend to move in the soil column with water.
81 This ideotype consists of highly gravitropic, vertically oriented roots that grow deep in the
82 soil column and develop large amounts of aerenchyma, which reduces the overall metabolic
83 cost of the root system³. Other nutrients, like phosphorus, which have limited water solu-
84 bility and are tightly bound to organic matter, usually accumulate in the top layers of soil
85 and favor root systems that are more highly branched and shallow. The low-phosphorus
86 ideotype effectively increases root exploration at the top layers of soil³. Modeling of root
87 system variables shows that optimum architecture for nitrogen and phosphorus uptake are
88 not the same⁹ and suggests tradeoffs that may affect the evolution of root architecture as a
89 population adapts to a particular environmental niche.

90 Clearly, understanding the architecture of root systems and how environmental conditions
91 alter root developmental programs is important for understanding adaptive mechanisms of
92 plants and for identifying the molecular-genetic basis for different response programs. In
93 addition, root systems have complexity beyond their architecture that needs to be incorpo-
94 rated into our understanding of plant-environment interactions. Primary and lateral roots
95 exhibit different stress response programs in *Arabidopsis*² and may play specialized roles
96 in water and nutrient uptake. Thus, it is important to develop methods that allow for a
97 multidimensional characterization of the root system that includes growth, signaling, and
98 interactions with other organisms. Furthermore, physiological parameters that affect whole
99 plant responses to the environment, such as transpiration, are likely integrated into such
100 processes, thus requiring a more holistic approach to studies of root function.

101 Based on these considerations we have developed a new root imaging platform, Growth
102 and Luminescence Observatory for Roots (GLO-Roots), which allows root architecture and

103 gene expression to be studied in soil-grown plants. GLO-Roots is an integrated system
104 composed of custom growth vessels, luminescent reporters and imaging systems. We use
105 rhizotrons that have soil volumes equivalent to small pots and support growth of Arabidopsis
106 from germination to senescence. To visualize roots, we designed plant-codon optimized
107 luciferase reporters that emit light of different wavelengths. To visualize reporter expression,
108 plants are watered with a dilute luciferin solution and imaged afterwards. We have built
109 a custom luminescence imaging system that automatically captures images of rhizotrons
110 held vertically. The signal from each reporter is distinguished using band-pass filters held
111 in a motorized filter wheel, which enables automated acquisition of images from plants
112 expressing both structural and environmentally and developmentally responsive reporters.
113 We have also developed GLO-RIA (GLO-Roots Image Analysis), an ImageJ¹⁰ plugin that
114 allows for automated determination of root system area, convex hull, depth, width and
115 directionality, which quantifies the angle of root segments with respect to gravity. GLO-
116 RIA is also able to relate root system parameters to local root-associated variables such as
117 reporter expression intensity and soil-moisture content.

118 Overall GLO-Roots has great utility in presenting environmental stimuli to roots in phys-
119 iologically relevant ways and provides tools for characterizing responses to such stimuli at
120 the molecular level in whole adult root systems over broad time scales.

121 **Box 1.**

122 All resources for GLO-Roots, including the user manual, the latest software downloads, the
123 source code, the original raw data used in the manuscript and sample images can be found
124 on https://github.com/rr-lab/glo_roots.

125 **Results**

126 We have developed an integrated platform for growing, imaging and analyzing root growth
127 that provides advances in physiological relevance and retains the ability to visualize aspects

¹²⁸ of root biology beyond structure.

¹²⁹ **The GLO-Roots platform**

¹³⁰ GLO-Roots is comprised of four parts: i) growth vessels called rhizotrons that allow plant
¹³¹ growth in soil and root imaging; ii) luminescent reporters that allow various aspects of
¹³² root biology to be tracked in living plants; iii) luminescence imaging system designed to
¹³³ automatically image rhizotrons; iv) GLO-RIA, an image analysis suite designed to quantify
¹³⁴ root systems imaged using GLO-Roots.

¹³⁵ **Plant growth system** GLO-Roots utilizes custom designed growth vessels classically
¹³⁶ known as rhizotrons, which hold a thin volume of soil between two sheets of polycarbonate
¹³⁷ plastic. Acrylic spacers provide a 2-mm space in which standard peat-based potting mix
¹³⁸ is added. Black vinyl sheets protect roots from light and rubber U-channels clamp the
¹³⁹ rhizotron materials together. Plastic racks hold the rhizotrons vertically and further protect
¹⁴⁰ the roots from light. Rhizotrons and rack are placed in a black tub and water are added, to
¹⁴¹ a depth of about 2 cm, at the bottom to maintain moisture in the rhizotrons during plant
¹⁴² growth. The volume of soil in the rhizotrons (100 cm^3) is similar to small pots commonly
¹⁴³ used for Arabidopsis and supports growth throughout the entire life cycle (Fig 1A-C and
¹⁴⁴ Supplement 1).

¹⁴⁵ To determine how the biology of plants grown in rhizotrons compares to other standard
¹⁴⁶ growth systems, we utilized high-throughput qRT-PCR to study how these conditions af-
¹⁴⁷ fect expression of 77 marker genes in root and shoot samples. These genes were curated
¹⁴⁸ from the literature and belong to a wide array of biological pathways including nutrient
¹⁴⁹ acquisition, hormone and light response and abiotic stress. Whole roots and shoot samples
¹⁵⁰ were collected at the end of the light and dark cycles (16 hour light, 8 hours dark) from
¹⁵¹ plants grown in rhizotrons, pots, and petri dishes with two different media compositions (1X
¹⁵² Murashige and Skoog basal salts (MS), 1% sucrose or 0.25X MS, no sucrose). Principal com-
¹⁵³ ponent analysis of the gene expression values showed a separation of soil and gel-grown root

systems in the the first principal components (Figure 1-figure supplement 1A). We observed enhanced expression of genes associated with light-regulated pathways (flavonoid biosynthesis: *FLAVINOL SYNTHASE1*, *FLS1*, *CHALCONE SYNTHASE*, *CHS*), (photosynthesis: *RUBISCO SUBUNITS1A*, *RBCS1A CYCLOPHILIN 38*, *CYP38*), which is expected due to the exposure of gel-grown roots to light. In addition, genes associated with phosphorus nutrition (*LOW PHOSPHATE RESPONSE1*, *LPR1*, *PHOSPHATE STARVATION RESPONSE1*, *PHR1*) were among others (Figure 1-figure table supplement 1) expressed predominantly in soil-grown roots, suggesting differences in nutrient availability between the different growth systems Interestingly, shoot samples where not clearly distinguished by growth media and, instead, time of day had a greater effect (Figure 1-Supplement 2). These data suggest root systems may be particularly sensitive to media conditions and indicate that rhizotron-grown root systems more closely approximate the biology of a pot-grown plant than standard gel-based media. Shoot weight and primary root length were significantly reduced for gel-grown plants compared to rhizotron- or pot-grown plants suggesting significant differences in the biology of plants grown under these conditions (Figure 1-figure supplement 1B-C). While the 2 mm depth of the soil sheet is 10 to 20 times the average diameter of an Arabidopsis root (between 100-200 microns), we evaluated whether rhizotron-grown plants exhibited any obvious stress as a consequence of physical constriction. We compared traits of plants growing in vessels that hold similar volumes of soil but in different volumetric shapes. The number of lateral roots was significantly lower in pot and cylinder-grown plants compared to rhizotron-grown plants (Figure 1-figure supplement 1D) whereas primary root length of rhizotron and cylinder-grown plants was significantly greater than pot-grown plants (Figure 1-figure supplement 1E). No significant differences in shoot area were observed between the three systems (Figure 1-figure supplement 1-data). Thus, these data do not support the hypothesis that rhizotron-grown plants experience physical constriction greater than other vessels holding the same volume of soil.

Generation of transgenic plants expressing different luciferases Arabidopsis roots cannot easily be distinguished from soil using brightfield imaging due to their thinness and

translucency (Figure 1-figure supplement 3); thus, reporter genes are needed to enhance the contrast between the root and their environment. Luciferase is an ideal reporter to visualize roots: 1) unlike fluorescent reporters, luciferase does not require high-intensity excitation light, which could influence root growth, 2) peat-based soil (a type of histosol) exhibits no autoluminescence but does autofluoresce at certain excitation wavelengths similar to GFP (Figure 1-figure supplement 3), 3) while GFP is very stable, and thus not as suitable for imaging dynamic transcriptional events, the luciferase enzyme is inactivated after catabolism of luciferin, making it ideal for studying processes such as environmental responses. A considerable number of luciferases have been developed that emit light spanning different regions of the visible spectrum, but their utilization has been limited to studies in animals (Table 1).

To determine the efficacy of using luciferase to visualize roots in soil, we codon optimized sequences of *PpyRE8*, *CBGRed*, *LUC2*, and *CBG99* for Arabidopsis expression. In addition, nanoLUC and venus-LUC¹¹ were utilized. Constitutive luciferase expression was driven in plants using the *UBIQUITIN 10* (*UBQ10*) or *ACTIN2* (*ACT2*) promoter using vectors assembled through a Golden-Gate cloning system¹². Plants homozygous for a single locus T-DNA insertion were evaluated for in vivo emission spectra and luminescence intensity (Fig 1D). All the evaluated luciferases use D-luciferin as a substrate facilitating the simultaneous imaging of different luciferases except nanoLUC, which uses a proprietary substrate furimazine. In general, luciferases with red-shifted emission spectra were less intense than the green-shifted luciferases (Fig 1D). LUC2o showed an emission maximum at 580 nm and a minor peak at 620 nm while CBG99o lacks the minor peak.

GLO1: a semi-automated luminescence imaging system for rhizotrons Luminescence imaging systems commercially available for biomedical research are usually optimized for imaging horizontally held specimens or samples in microtiter plates. Placing rhizotrons in this position would induce a gravitropic response in plants. Working with Bioimaging Solutions (San Diego, CA) we designed and built a luminescence imaging system optimized for rhizotron-grown plants. GLO1 (Growth and Luminescence Observatory 1) uses two

210 back-thinned CCD cameras (Princeton Instruments, USA) to capture partially-overlapping
211 images of rhizotrons while a motorized stage automatically rotates the rhizotron to capture
212 images of both sides (Fig 1E). A composite image is generated from the images of each side;
213 Fig 1F shows that approximately half of the root system is revealed on each side with few
214 roots being visible on both sides. Apparently, the soil sheet is thick enough to block portions
215 of the root system but thin enough to ensure its continuous structure can be compiled from
216 opposite face views. We tested the ability of GLO1-generated images to reveal complete
217 root systems by manually quantifying the number of lateral roots in excavated root systems
218 of 8 different plants and testing these results against estimates of lateral root number from
219 images of the same plants visually inspected by 4 different persons. These comparisons
220 revealed good correlation ($(R^2 = 0.974)$) between actual lateral root counts and image-based
221 estimation, indicating GLO1-generated root images provide an accurate representation of
222 the in soil root system.

223 Continuous addition of luciferin did not have any significant effect on shoot weight or primary
224 root length (Figure 1-figure supplement 4). After luciferin addition, luminescence signal
225 could be reliably detected in root systems for up to 10 days, depending on the developmental
226 state of the plant.

227 **GLO-RIA: GLO-Roots Image Analysis** We developed a set of image analysis algo-
228 rithms that were well suited for the complex root systems that GLO-Roots is able to capture.
229 GLO-RIA (Growth and Luminescence Observatory Root Image Analysis) is an ImageJ plu-
230 gin divided in two modules. The first module (RootSystem) performs four different types of
231 analysis: i) a local analysis that detects all root particles in the image and computes their
232 position, length and direction; ii) the global analysis performs a root system level analysis
233 and computes the total visible surface, convex hull, width and depth; iii) the shape analysis
234 uses Elliptic Fourier Descriptors or pseudo-landmarks similarly to RootScape¹³ to perform
235 a shape analysis on the root system iv) the directionality analysis computes the mean di-
236 rection of root particles in a root system (either on the full image or by user-defined region
237 of interest in the image). These four analysis methods are fully automated by default, but

238 can be manually adjusted if needed. The second module of GLO-RIA (RootReporter) was
239 specifically designed for the analysis of multi-layered images such as combinations of gene
240 reporter, root structure and soil moisture. Shortly, the plugin works as follow: i) detection
241 of the gene reporters and the structure reporters in their respective images; ii) if needed, a
242 manual correction can be performed to correct the automated detection; iii) gene reporters
243 are linked with the soil water content and the structure reporters, based on their proximity;
244 iv) gene reporter intensity (either absolute or normalized using the structural reporter) is
245 computed; v) all data are exported and saved to a RSML datafile¹⁴. Gene and structure
246 reporters can be followed across different time and space points. Using an object oriented
247 approach, great care has been taken to facilitate the user interactions on the different images
248 to streamline the analysis process. Table 2 shows a list of root system features extracted
249 using GLO-RIA. GLO-RIA does not currently have the ability to reconstruct the root archi-
250 tecture in itself (topological links between roots). This is a challenge for analyzing images
251 captured by GLO-Roots since soil particles cause disruption of root segments.

252 **Continuous imaging of root growth**

253 The size of our rhizotrons enables undisturbed root system development (before roots reach
254 the sides or the bottom of the rhizotron) for about 21-23 days for the Col-0 accession
255 growing under long day conditions (Figure 2); however root traits such as directionality
256 can be observed until later stages of plant development. See 35 DAS root system and
257 directionality in Figure 2A-B. An example of a time series spanning 11 to 21 days after
258 sowing (DAS) of Col-0 roots expressing *ProUBQ10:LUC2o* is shown in Fig 2A and [Video 1](#)
259 with a color-coded time projection shown in Fig 2C. Directionality analysis (Fig 2B) shows
260 a progressive change in root system angles from 0 ° (vertical) to 45 ° as lateral roots take
261 over as the predominant root type. Figure 2D shows the evolution over time of several root
262 traits that can be automatically captured by GLO-RIA (depth, width, area) and others
263 that can be manually quantified (primary root growth rate or number of lateral roots per
264 primary root).

265 Root system architecture of different *Arabidopsis* accessions.

266 The study of natural variation for root system architecture and root traits is a powerful
267 approach for understanding adaptive strategies plants use to cope with environmental change
268 and for identifying the genetic basis for such differences. In *Arabidopsis*, Quantitative Trait
269 Locus (QTL) and Genome-Wide Association Studies (GWAS) have led to the identification
270 of genes affecting root development¹⁵. However, traits are usually measured in seedlings
271 less than 2 week old. Selective pressures that affect allele frequencies in a population likely
272 act on genes that affect root system traits at later stages of the plant life cycle, as well.
273 As a proof of concept to estimate the utility of our root imaging system to phenotype
274 adult root system traits, we transformed a small set of accessions (Bay-0, Col-0 and Sha)
275 with the *ProUBQ10:LUC2o* reporter and quantified RSA at 22 DAS (Fig 3A-C). GLO-RIA
276 analysis of these root systems identified several root traits that distinguish Col-0, Bay-0
277 and Sha. Directionality analysis revealed an abundance of steep-angle regions in the root
278 system of Bay while Sha showed an abundance of shallow-angled regions and Col-0 was
279 intermediate (Fig 3D). Bay-0 shows the deepest and narrowest root system leading to the
280 highest depth/width ratio while Sha has the widest root system (Fig 3E). Other root traits
281 such as root system area and the vertical center of mass also showed significant differences
282 (Figure 3-figure supplement 1B). Broad sense heritability values for depth (96.3), area (92.0),
283 depth/width (97.8), width (95.7) and vertical center of mass (95.0) were all higher than
284 90%. To capture the richness of root architecture shape, we used GLO-RIA to extract
285 pseudo-landmarks describing the shape the root system to perform PCA analysis. The first
286 principal component separates Col-0 and Sha plants from Bay-0 ones capturing root systems
287 that vary in the distribution of widths along the vertical axis. (Fig 3F). While Bay-0 shows
288 an homogenous distribution of widths along the vertical axis, Sha and Col-0 are much wider
289 at the top than in the bottom. PC2 seems to be capturing a relationship between width at
290 the top and depth, slightly separating Sha root systems which are wide at the top and deep
291 from Col-0 root systems which are wide but not as deep as in Sha. Using shape information
292 extracted from EFDs we can distinguish the three different accesions using PCA analysis

²⁹³ (Fig 3G)

²⁹⁴ **GLO-Roots for Brachypodium and Tomato**

²⁹⁵ To examine the general applicability of the GLO-Roots system for other species, we intro-
²⁹⁶ duced LUC2o-expressing reporters into the model grass *Brachypodium distachyon* and the
²⁹⁷ crop plant *Lycopersicon esculentum* (tomato). Brachypodium is well suited to the GLO-Root
²⁹⁸ system because, like Arabidopsis, its small size allows mature root systems to be studied in
²⁹⁹ relatively small soil volumes^{16,17}. *LUC2o* driven by the *ZmUb1* promoter was introduced into
³⁰⁰ Brachypodium using the pANIC vector¹⁸. Brachypodium roots showed a distinct architec-
³⁰¹ ture from Arabidopsis marked by prolific development of secondary and tertiary lateral roots
³⁰² (Fig 4A). This is consistent with other studies that show that Brachypodium has a typical
³⁰³ grass root system¹⁷. Comparison of root system development in rhizotrons with gel-based
³⁰⁴ media showed that root growth is higher in soil than in plates (Figure 4-figure supplement
³⁰⁵ 1). Previous work has suggested that auxin levels in Brachypodium roots is sub-optimal for
³⁰⁶ growth¹⁹. Pacheco-Villalobos and colleagues suggest that, in Brachypodium, and contrary
³⁰⁷ to what happens in Arabidopsis, ethylene represses *YUCCA* reducing the synthesis of auxin.
³⁰⁸ The reduced growth that we observe in plates and the high levels of ethylene that build up
³⁰⁹ in sealed plates²⁰ would support this mechanism.

³¹⁰ Tomato plants were transformed with *Pro35S:PPyRE8o* and *ProeDR5rev:LUC2* reporters.
³¹¹ The plants showed more rapid growth than Arabidopsis or Brachypodium and required fer-
³¹² tilizer to prevent obvious signs of stress (reduced growth, anthocyanin accumulation). Root
³¹³ systems were imaged from 17 DAS plants. Roots showed less branching than Arabidopsis
³¹⁴ but many presumptive lateral root primordia marked by DR5-expression (Fig 4C-D). These
³¹⁵ results show that the GLO-Roots method can be applied to study root systems of plants
³¹⁶ and will likely be useful for studying root systems of other small to medium sized model
³¹⁷ plants and for early stages of larger crop plants.

**318 Spectrally distinct luciferases enable gene expression patterns, characterization
319 of root system interactions and microbial colonization.**

320 We tested whether spectrally distinct luciferase reporters would enable additional information
321 besides root architecture to be captured from root systems. Luciferase reporters have
322 been commonly used to study gene expression and these resources can potentially be utilized
323 to study these regulatory events in soil-grown roots. We transformed *ProACT2:PpyRE8o*
324 into two well studied LUC reporter lines: the auxin response reporter line *ProDR5:LUC*²¹
325 (Figure 5A-B) and the Reactive Oxygen Species (ROS) response reporter *ProZAT12:LUC*²²
326 (Figure 5C-D). We implemented in GLO-RIA an algorithm that semi-automatically identifies
327 gene reporter signal and associates this object to the corresponding root structure segment.
328 A graphical representation of the results obtained with Root Reporter can be observed in
329 Figure 5E. Reporter intensity values along the first 5 mm of root tips can also be observed in
330 Figure 5-figure supplement 1. We then took advantage of our ability to constitutively express
331 two spectrally different luciferases and imaged the overlapping root systems (one expressing
332 *ProUBQ10:LUC2o* and the other *ProACT2:PPy RE8o*). Root systems were distinguishable
333 using this system (Figure 5-figure supplement 2); measurements of root system area did not
334 reveal a significant effect on root growth when two plants were grown in the same rhizotron,
335 however further studies are warranted (Figure 5-figure supplement 2) The GLO-Roots sys-
336 tem uses non-sterile growth conditions, which allows complex biotic interactions that may
337 affect responses to the environment. Bacteria themselves can be engineered to express lumi-
338 nescent reporters through integration of the LUX operon, which results in luminescence in
339 the blue region of the spectrum and is thus compatible with the plant-expressed luciferase
340 isoforms we have tested. *Pseudomonas fluorescens* CH267²³, a natural Arabidopsis root
341 commensal, was transformed with the bacterial LUX operon and used to inoculate plants.
342 Thirteen days after inoculation we were able to observe bacterial luminescence colocalizing
343 with plant roots. *P. fluorescens* did not show an obvious pattern of colonization at the root
344 system scale level. As a proof-of-principle test of the multi-dimensional capabilities of the
345 GLO-Roots system we visualized both *LUC2o* and *PPyRE8o* reporters in plants and the

³⁴⁶ LUX reporter in bacteria in the same rhizotron (Figure 5-figure supplement 3).

³⁴⁷ **Adaptive changes in root system architecture under water deprivation, phos-**

³⁴⁸ **phorus deficiency and light** To test the utility of the GLO-Roots system to understand
³⁴⁹ response of root systems to environmental stimuli we tested the effects of light and condi-
³⁵⁰ tions that mimic drought and nutritional deficiency. To examine the effects of light exposure
³⁵¹ on the root architecture, the black shields, which normally protect the soil and roots from
³⁵² light, were removed from the top half of the rhizotrons 10 DAS. Using directionality analysis
³⁵³ we detected a significant increase in the steepness of roots only in the light exposed region of
³⁵⁴ the rhizotron, while the lower shielded region showed no difference. (Fig 7-figure supplement
³⁵⁵ 3A-B and Fig 7-figure supplement 4). Light can penetrate the top layers of soil²⁴ and it
³⁵⁶ has been proposed to have a role in directing root growth specially in dry soils²⁵ through
³⁵⁷ the blue light receptor *phot1*. Root directionality was not significantly different between
³⁵⁸ light and dark-treated roots of the *phot1/2* double mutant suggesting that blue light per-
³⁵⁹ ception is necessary for this response^{25,26} (Fig 7-figure supplement 3B-lower panel). These
³⁶⁰ data highlight the strong effects of light on root system architecture²⁷, which GLO-Roots
³⁶¹ rhizotrons are able to mitigate.

³⁶² Plants grown in low-P soil showed a significant increase in the width-depth ratio of the root
³⁶³ system compared to plants grown in P-replete soil, as determined using the automated root
³⁶⁴ system area finder in GLO-RIA (Fig 7-figure supplement 2A-B). Plants under P deficiency
³⁶⁵ showed an increase in the ratio between root-shoot area (Fig 7-figure supplement 2C) and
³⁶⁶ higher investment of resources in the development of the root system at the expense of shoot
³⁶⁷ growth (Fig 7-figure supplement 2D). Root systems of control and P-deficient plants showed
³⁶⁸ no significant differences in directionality at 22 DAS but at 27 DAS, roots were more hori-
³⁶⁹ zontally oriented in P-deficient plants (Fig 7-figure supplement 2E). The observed changes in
³⁷⁰ root architecture are consistent with root system ideotypes that improve phosphorus uptake
³⁷¹ efficiency.

³⁷² GLO-Roots is especially well suited for studying water-deficit (WD) responses. First, shoots

373 are exposed to the atmosphere and vapor pressure deficit (VPD) is maintained at levels that
374 allow for transpiration of water from the shoot. Second, soil in rhizotrons is exposed to air
375 at the top and dries basipetally (from the top-down); drying soil increases the volume
376 occupied by air and reduces contact of root with liquid water, all of which are similar to
377 changes in soil expected in the field during WD. Finally, as peat-based soil dries, its optical
378 properties change, allowing moisture content to be approximated from bright-field images.
379 We took advantage of the change in gray-scale pixel intensity to construct a calibration
380 curve (Figure 6-figure supplement 1) that quantitatively relates gray-scale pixel intensity to
381 moisture content (Fig 6A); water content can be color coded in images with appropriate
382 look up tables (Fig 6B). Soil color was not affected by the presence or absence of roots
383 (Figure 6-figure supplement 2). Using this approach, water content in a rhizotron can be
384 mapped and visualized in 2D (Fig 6C-D). In the example shown, we can observe that a 22
385 DAS Bay-0 plant depleted soil-moisture content locally around the the root system (Figure
386 6E).

387 We performed several trials to simulate WD in our growth system. Plants were germinated,
388 grown under control conditions then transferred to 29°C and standing water removed from
389 the container holding the rhizotrons starting at 9 DAS or 13 DAS. Elevated temperature
390 combined with water deficit is a common stress that modern crops varieties are poorly
391 adapted to, thus highlighting the importance of examining this combined treatment^{28,29}.
392 Plants were maintained in this WD regime until 22 DAS when luciferin was added and the
393 plants were imaged. At 13 DAS, lateral roots near the soil surface are already emerged
394 ([Video 1](#), Figure 2A). After 9 days of water deficit treatment, lateral roots showed an in-
395 crease in gravitropism leading to the development of a root system that was deeper, more
396 vertically oriented and with more tertiary roots (Fig 7A). Roots of Bay-0 plants showed
397 similar responses though the extent of change was less pronounced since Bay-0 roots are
398 normally more vertically oriented (Fig 7B). Plants transferred at 9 DAS showed less lateral
399 root development in the top layer of soil (Fig 7E). At this time point, lateral roots start to
400 emerge ([Video 1](#)) and early drought may lead to growth quiescence or senescence. Careful
401 examination of roots in these regions showed evidence of small lateral root primordia pop-

402 ulating the primary root (Figure 7F). After 24 h of re-watering (Figure 7G) these lateral
403 root primordia reinitiated growth (Figure 7H).

404 Time-lapse imaging of the water deficit response showed that changes in root growth direc-
405 tion occurred ahead of the dry soil front [Video 3](#). Using GLO-RIA we were able correlate
406 water moisture contents with local orientation of the root segments. With this approach we
407 observed that root segments in dryer areas of rhizotron grew at steeper root angles (Figure
408 8) than roots in growing in well watered regions, though lateral root angle in wetter regions
409 was also affected. These data suggest that local and systemic signaling is likely involved in
410 redirecting lateral roots deeper during the simulated drought treatments tested here.

411 We also grew plants under WD at control temperatures or under WW conditions at elevated
412 temperature to test the effects of these individual stresses on root architecture. We observed
413 that both conditions were sufficient to induce a change in root directionality indicating that
414 the plant uses similar mechanisms to avoid heat and water-deficit associated stresses (Figure
415 7-figure supplement 1). We next asked which regulatory pathways controlled the observed
416 changes in lateral root directionality during simulated drought. Hydrotropism is a known
417 environmental response that directs root growth towards wet regions of soil. MIZ1 is an
418 essential regulator of hydrotropism; however *miz1* mutants had no significant effect on water
419 deficit-induced changes in root directionality, compared to wild type (Fig 7C), indicating
420 that this response was distinct from hydrotropism. Auxin is an important mediator of
421 gravitropism and auxin treatment causes lateral roots to grow more vertically⁷. Consistent
422 with this role for auxin, mutant plants with loss of function in the auxin receptor TIR1, did
423 not show changes in the root system directionality between WW and WD conditions (Fig
424 7D).

425 **Discussion**

426 **GLO-Roots enables a multi-dimensional understanding of root biology**

427 Recent studies of root systems has emphasized structural attributes as important contrib-
428 utors of root system function. Indeed, studies examining the role of genetic variants in
429 tolerating abiotic stress have demonstrated the importance of such characteristics. Roots,
430 however, are highly diverse in the biology they perform and a multi-dimensional understand-
431 ing of root systems, which incorporates differences in signaling, metabolism and microbial
432 association as well as structure, may provide a clearer understanding of the degree to which
433 sub-functionalization of the root system plays a role in important processes such as acclima-
434 tation and efficient resource acquisition.

435 We have developed tools in GLO-Roots that allow for tracking multiple aspects of soil
436 physicochemical properties and root biology simultaneously. Using GLO-Roots, we are able
437 to map in 2D coordinates soil physical properties such soil moisture together with root ar-
438 chitecture traits such as directionality, growth rates and gene expression levels. All this
439 information is aggregated in layers for each x, y coordinate. Using GLO-RIA we integrate
440 this multilayer information, leveraging our ability to simultaneously and seamlessly inves-
441 tigate root responses to environmental stimuli such as soil moisture content. Luciferase
442 isoforms that emit light at different wavelengths allow for constitutive and regulated pro-
443 moters to be studied together. Introduction of luciferase reporters into microbes provides
444 an additional layer of information that provides a readout on the association between or-
445 ganisms and how this might be affected by environmental conditions. The flexibility of the
446 GLO-Roots system may enable additional dimensionality to our understanding of root biol-
447 ogy. Other physical properties such as CO₂ or pH mapping in rhizotrons have already been
448 enabled by using planar optodes³⁰. It may be possible to engineer LUX-based reporters
449 in microbes that are responsive to extracellular metabolites, creating microbial biosensors,
450 and integration of such tools may enable root-exudation and nutrition to be analyzed in
451 soil. Split-Luciferase reporters have been engineered that allow bi-molecular interactions to
452 be studied. Finally, molecular sensors analogous to FRET sensors, termed BRET-sensors³¹,

453 may allow metabolite tracking dynamically through the root system. With additional inno-
454 vation in the development of luciferase reporters, the GLO-Roots systems will likely expand
455 the repertoire of biological processes that can be studied over an expanded range of devel-
456 opmental time points and environmental conditions.

457 **Enhanced root growth and gravitropism may constitute an avoidance mechanism**
458 **used during drought**

459 It has been proposed that plants with steep root systems will be better able to tap into deep
460 water resources and thus perform better under water deprivation. For example in rice, the
461 IR64 paddy cultivar shows shallow root systems in upland fields whereas Kinandang Patong,
462 an upland cultivar, is deeper rooting⁸. Plants maintain a number of regulatory pathways that
463 mediate changes in physiology during WD. Enhanced growth of root systems has been well
464 characterized in field-grown plants; however this has not been recapitulated in studies of gel-
465 grown Arabidopsis plants. Thus, it has been unclear whether Arabidopsis simply responds
466 to WD differently. Our results here show that Arabidopsis does indeed maintain a classical
467 WD response that expands the root system and directs growth downward. Interestingly,
468 under our stress regime, we did not observe a significant decrease in the relative water
469 content of shoot tissues (Figure 7-figure supplement 5), suggesting that the changes in root
470 architecture were sufficient to provide access to deep water and prevent dehydration. Such
471 changes in root growth are likely regulated through systemic and local signaling that involve
472 auxin signaling but acts independently of known pathways that control moisture-directed
473 root growth.

474 **Perspectives and Conclusions**

475 Understanding plant biology requires a sophisticated understanding of how environmental
476 stimuli affect the form and function of plants as well as an understanding of how physiological
477 context informs such responses. Environmental conditions are at least as complex as the
478 plants they affect. Plant roots are exposed to a variety of environmental signals that change

479 in time and space at very different scales that are integrated at the whole plant system. It is
480 an important challenge in biology to develop methods of growing and studying plants that
481 present such stimuli in a manner that the plant is likely to encounter in nature. After all, the
482 plants we study have evolved to survive through mechanisms that have been selected, over
483 evolutionary time, in nature. It will be interesting for future studies to determine how other
484 environmental stimuli affect root growth using GLO-Roots and whether these responses
485 differ between accessions of Arabidopsis. Identification of the genetic loci responsible for
486 phenotypic variation in adult root phenotypes may identify the molecular basis for adaptive
487 variation that exists in this species and potentially identify loci that are useful for breeding
488 efforts needed for the next green revolution.

489 Materials and methods

490 Growth system

491 **Rhizotrons and growth system fabrication.** Rhizotrons are composed of two sheets of
492 1/8" abrasion resistant polycarbonate plastic (Makrolon AR (R)) cut to size using a water
493 jet (AquaJet LLC, Salem, OR), two acrylic spacers cut using a laser (Stanford Product
494 Realization Lab), two rubber U-channels cut to strips 30 cm long ([McMaster Carr part](#)
495 [# 8507K33](#)) and two sheets of black 0.030" thick polypropylene sheets ([McMaster Carr](#)
496 [part # 1451T21](#)) cut with a straight-edge razor blade. Rhizotron designs were drafted in
497 Adobe Illustrator (Adobe, San José, CA). The blueprints of all the parts are provided in
498 Supplement 1. The top edge of each polycarbonate sheet was painted with black 270 Stiletto
499 nail polish (Revlon, New York, NY).

500 **Boxes and holders.** Rhizotrons are held vertical during plant growth in a custom rack sys-
501 tem composed of two sheets of 1/4" black acrylic plastic cut with slots for eleven rhizotrons
502 using a laser, four 3/8" PVC rods ([McMaster Carr part # 98871a041](#)) secured with PVC
503 nuts ([McMaster Carr part # 94806a031](#)) to hold the acrylic sheets horizontal. The rack is
504 placed inside a 12" x 12" x 12" black polyethylene tank ([Plastic Mart part # R121212A](#)).

505 **Rhizotron preparation** The procedure to construct a rhizotron with soil is as follows:
506 Two pieces of polycarbonate plastic are laid flat on a table with the spacers inserted. Using
507 an electric paint gun, a fine mist of water is applied to the bare polycarbonate sheets. Then,
508 using a 2 mm sieve (US Standard Sieve Series N° 10) a fine layer of PRO-MIX(r) PGX soil
509 (Premier Tech, Canada) is applied. Excess soil is discarded by gently tapping the plastic
510 against the table in a vertical position. Water is sprayed again onto the soil, then a second
511 layer of Pro-MIX is applied as before. For P deficiency experiments soil supplemented with
512 1 ml of 100 μM P-Alumina (control) and 0-P-Alumina (P deficient) was used. To prevent
513 the soil from falling out of the bottom opening, a 3 x 6 cm piece of nylon mesh is rolled into
514 a 1 cm wide tube and placed at the bottom side of the rhizotron. The spacers are removed
515 and replaced by clean spacers. The two faces of the rhizotron are carefully joined together
516 and two rubber U-channels slipped on to clamp all pieces together. Assembled rhizotrons
517 are placed into the rack inside the boxes and 500 mL of water is added to the box.

518 **Plant growth** *Arabidopsis thaliana* seeds were stratified for 2 d at 4 °C in Eppendorf tubes
519 with distilled water. Seeds were suspended in 0.1 % agar and 5 to 10 were sown using
520 a transfer pipette in the rhizotron. A transparent acrylic sheet was mounted on top of
521 the box and sealed with tape to ensure high humidity conditions that enable *Arabidopsis*
522 germination. Three days after sowing, the cover was unsealed to decrease humidity and
523 allow the seedlings to acclimate to a dryer environment. From 3 days after sowing (DAS)
524 to the time the first true leaves emerged, it was critical to ensure that the top part of the
525 rhizotron remained humid for proper germination of the plants. Between three and five DAS
526 the rhizotrons were thinned leaving only the number plants required for that experiment,
527 typically one, except for experiments examining root-root interactions. Unless otherwise
528 stated, all the experiments presented here, treatments were started 10 DAS. Plants were
529 grown under long day conditions (16 h light / 8 h dark) using 20–22 °C (day/night) and
530 150 $\mu\text{E m}^{-1} \text{s}^{-1}$. Two types of growth environments were used for experiments. A walk-in
531 growth chamber with fluorescent lightning and a growth cabinet with white LED lights.
532 Relative water content measurements were done as previously described³²

533 **qRT-PCR analysis.**

534 Seeds were surface sterilized as described before² and grown in rhizotrons, 100 cm³ pots, or
535 on two types of 1% agar (Duchefa) media containing either 1x MS nutrients (Caisson) and 1%
536 Sucrose, (termed ms media) or ¼x MS nutrients only (termed ms25 media). Both media were
537 buffered using 0.5 g/L MES and pH was adjusted to 5.7 with KOH. All plants were grown
538 together in a growth cabinet with LED lights under long day conditions (16h day/8h night).
539 Root and shoot tissue was collected separately from individual plants at the end of the day
540 (1 hour before the lights shut off) and at the end of the night (1 hour before lights came on).
541 Three biological replicates were collected for each condition. RNA was extracted using the
542 Plant RNA MiniPrepTM kit (ZYMO Research) according to manufacturer's instructions
543 with on-column DNase treatment (Qiagen). cDNA was made using the iScript Advanced
544 cDNA Synthesis for RT-qPCR kit (Bio-Rad) from 200 ng of total RNA. qRT-PCR was
545 performed using a Fluidigm BioMarkTM 96.96 Dynamic Array IFC with the EvaGreen®
546 (Bio-Rad) fluorescence probe according to the Fluidigm Advanced Development Protocol
547 number 37. For the analysis, all the reactions with no amplification (Ct =999) were either
548 removed (if the other technical duplicate amplified) or set to the maximal Ct for that assay
549 type. The two technical replicates were then averaged and dCt values calculated using
550 AT3G07480, AT4G37830, At1g13320 and At1g13440 as reference internal controls. PCA
551 plots were generated with Devium Web³³ using log dCt values. Primers used are listed in
552 file Supplement 8.

553 **Biological components**

554 **Codon optimization of luciferases.** The following luciferases that emit light at different
555 wavelengths were codon optimized for *Arabidopsis* (Genscript, Piscataway, NJ): LUC2: a
556 yellow improved version (Promega, Madison, WI) of the original *Photinus pyralis* (firefly)
557 LUC.

- 558 • Ppy RE8: a red variant³⁴ of the *P. pyralis* thermostable variant Ppy RE-TS³⁵.

- 559 • CBG99: a green variant (Promega, Madison, WI) from yellow click beetle (*Pyrophorus*
560 *plagiophthalmus*) luciferases.
- 561 • CBR: a red variant (Promega, Madison, WI) from yellow click beetle.

562 **Non-optimized luciferases.** We also used the following non-optimized luciferases:

- 563 • nanoLUC: a blue luciferase isolated from a deep sea shrimp³⁶.
- 564 • venusLUC2: a venus-LUC2 fusion reported to show higher luminescence output than
565 LUC2¹¹.
- 566 • A transposon containing the bacterial luciferase-containing LUX operon was inte-
567 grated into the *Pseudomonas fluorescens* CH267²³ genome by conjugation with *E.*
568 *coli* SM10 *pir* containing pUT-EM7-LUX³⁷ and used to track root microbe coloniza-
569 tion. For inoculation 9 DAS plants were inoculated with 2 mL of an overnight bacterial
570 culture resuspended in 10 mM MgSO~4 and diluted to 0.01 OD.

571 **Generation of single-reporter transgenic plants.** We generated transcriptional fu-
572 sions of all luciferases to constitutive promoters to examine the activity level and emission
573 spectrum of each isoform. The *attL1-attL2** entry clones containing plant-codon optimized
574 coding sequence of *LUC2*, *PpyRe8*, *CBG99* and *CBR* were synthesized by Genscript. A
575 DNA fragment including the *UBQ10* promoter region and first intron was amplified from
576 Col-0 genomic DNA with primers incorporating the attB1, attB4 combination sites at the 5'
577 and 3' respectively. The PCR product was then introduced into pDONR™ P4-P1R (Invitro-
578 gen) through a classic Gateway BP-reaction. The resulting plasmid, the *attL1-attL2* entry
579 clones with luciferase sequences, an empty *attR2-attL3** entry clone and the destination
580 vector dpGreenmCherry² were used to construct *ProUBQ10:LUC2o*, *ProUBQ10:PpyRE8o*,
581 *ProUBQ10:CBG99o* and *ProUBQ10:CBRo* through Gateway LR reactions. The destination
582 vector *dpGreenmCherry* contains a plasma membrane-localized mCherry coding sequence
583 driven by the 35S promoter and is used as a selectable marker of transformation at the

584 mature seed stage². We used Golden Gate cloning and the destination vectors that we had
585 generated before¹² for the following fusions: *ProUBQ10:nanoLUC2*, *ProUBQ10:venusLUC*,
586 *ProACT2:PpyRE8o*. Briefly, the different components of each construct were PCR ampli-
587 fied with complementary BsaI or SapI cutting sites, mixed with the destination vector in
588 a single tube, digested with either BsaI or SapI, ligated with T4 DNA ligase, then trans-
589 formed into *E. coli* Top10 cells and plated on LB antibiotic plates containing X-gal as pre-
590 viously described¹². Junction sites were confirmed by sequencing. We used pSE7 (Addgene
591 ID #: pGoldenGate-SE7: 47676) as the destination vector of the *ProUBQ10:nanoLUC2*,
592 *ProUBQ10:venusLUC* constructs and pMYC2 (Addgene ID #: pGoldenGate-MCY2: 47679)
593 as the destination vector for *ProACT2:PpyRE8o*. Maps of all the vectors can be found in
594 Supplement 8. *ProUBQ10:LUC2o* was transformed into Col-0, Bay and Sha accessions, the
595 *tir1-1*³⁸ mutant and the *miz1*³⁹ T-DNA insertion line (SALK_126928).

596 **Brachypodium distachyon** The *Arabidopsis* plant-codon optimized Luciferase gene,
597 *LUC2o*, was inserted into the monocot vector pANIC10 via Gateway cloning¹⁸. *Brachy-*
598 *podium distachyon* plants were transformed using the method of Vogel and Hill⁴⁰.

599 **Tomato** The transcriptional fusion *ProeDR5:LUC2* was generated by cloning the
600 *ProeDR5:LUC2* DNA fragment into the pBIB expression vector via restriction sites SalI
601 and Acc65I. The eDR5 promoter is an enhanced version of DR5 containing 13 repeats of
602 the 11-nucleotide core DR5 element⁴¹ and the pBIB expression vector contains an NPTII
603 resistance gene under the control of the NOS promoter for use as a selectable marker during
604 transformation. All tomato transformations were performed by the Ralph M. Parsons
605 Foundation Plant Transformation Facility (University of California, Davis).

606 **Generation of dual-reporter plants.** To generate dual-reporter plants expressing lu-
607 ciferase isoforms that emit light with divergent emission spectra we used *ProACT2:PpyRE8o*
608 as the root structural marker and ZAT12:LUC²² and DR5:LUC+²¹ lines that were trans-
609 formed with the *ProACT2:PpyRE8o* construct. All constructs were transformed using a

610 modified floral dip method as described in².

611 To make the dual color tomato plants, the *Pro35S:PpyRE8o* transcriptional fusion was
612 generated by putting the plant-codon optimized coding sequence described above into the
613 pMDC32 expression vector through a Gateway LR reaction. The pMDC32 vector con-
614 tains a hygromycin resistance gene under the control of the 35S promoter for use as a se-
615 lectable marker during transformation. This construct was transformed into the transgenic
616 *ProeDR5:LUC2* tomato line.

617 **In vivo emission spectra of plants constitutively expressing luciferase isoforms.**

618 To generate *in vivo* emission spectra of all constitutively expressed luciferases, seeds were
619 sterilized and sown on MS plates as described before². After 8 days, seedlings were treated
620 with a 100 µM luciferin solution, incubated at room temperature for 3 hours and imaged
621 using an IVIS Spectrum imaging system (Perkin Elmer, Waltham , MA) using 20 nm band-
622 pass emission filters at the following wavelengths (in nm: 490-510, 510-530, 530-550, 550-570,
623 570-590, 590-610, 610-630, 630-650, 650-670, 670-690, 690-710). Raw images were analyzed
624 using Fiji and *in vivo* emission spectra were constructed. The full emission spectra of LUX
625 and nanoLUC could not be constructed since the maximum of these two luciferases is below
626 the lower band pass filter that were available.

627 **Imaging system** We designed a custom imaging system (GLO1, Growth and Lumines-
628 cence Observatory 1) optimized for imaging dual-reporter luciferase expression in our custom
629 rhizotrons. The design was a joint effort with Bioimaging Solutions (San Diego, CA) who
630 also built the system and wrote the acquisition software that drives all the mechanical parts
631 of the system. The system is composed by two 2048 x 2048 PIXIS-XB cameras (Princeton
632 Instruments, Trenton, NJ) mounted on top of each other to capture two fields of view en-
633 compassing approximately two 15 x 15 cm areas corresponding to the top or bottom of the
634 rhizotron. The cameras are fitted with a Carl-Zeiss macro lens. A filter wheel with space
635 for four, 76.2 mm filters is positioned in front of the cameras and controlled by a stepper
636 motor allowing for automated changing of the filter wheel position. We used two -542/50

and 450/70- custom cut Brightline(R) band-pass filters (Semrock, Rochester, NY). In single color imaging mode, the filter wheel is operated without filters. Positioned in front of the filter wheel is a removable rhizotron holder mounted on a stepper motor. This stepper motor is also controlled by the GLO-1 software allowing automatic acquisition of images from both sides of the rhizotron sequentially. The whole imaging system is enclosed in a light-tight black box with a door that allows loading and un-loading of rhizotrons.

Plant Imaging Around 50 mL of 300 μ M D-luciferin (Biosynth, Itasca, IL) was added to soil at the top of the rhizotron. In general 5 min exposures were taken per rhizotron, per side, per channel. For daily imaging experiments, plants were imaged at dawn (+/- 1 hr) to reduce possible effects on diurnal rhythms of keeping plants in the dark during imaging.

Shoot images were taken using a Nikon D3100 camera.

Image Preparation Four individual images are collected: top front, bottom front, top back and bottom back. Using an automated [ImageJ macro](#), a composite image is generated as follows: 1)To correct for differences in background values between the two cameras the mean background value of each image is subtracted from 200; 2) images are rotated and translated to control for small misalignments between the two cameras; 3) the top and bottom images of each side are merged; 4) the back image is flipped horizontally; 5) the front and back images are combined using the maximum values. When dual color images are acquired this operation is repeated for each channel. The final images produced are 16-bit depth and 4096 x 2048 pixels. The scale of the images is 138.6 pixels per cm. Considering that an Arabidopsis roots is 100 μ m this results in 1.39 pixels across an Arabidopsis root.

GLO-RIA imageJ plug-in GLO-RIA uses a combination of existing tools to extract relevant root architecture features. Directionality is acquired using the [directionality plugin](#) from ImageJ. After the number of direction bins (we usually use bins of 2 $^{\circ}$) is defined by the user, a 5x5 sobel operator is used to derive the local gradient orientation. This orientation is then used to build a distribution of directions by assigning the square of the orientation

663 into the appropriate bin. Instead of representing the total counts at each orientation a
664 relative value is calculated by dividing the individual values at each bin by the total sum
665 of the histogram (and multiplying by 100). Similar algorithms have been used to quantify
666 dynamic changes in the plant cytoskeleton⁴².

667 The Elliptic Fourier Descriptors are aquired using the [Fourier Shape Analysis plugin](#) on
668 convex hull shape of the root system. Elliptic Fourier Descriptors have been used in numer-
669 ous studies to analyse variations in shapes, notably in leaves (e.g⁴³) The shape analysis is
670 inspired by RootScape¹³. Due to the absence of fixed, recognisable structures in root system
671 (that are required for the position of true landmarks), pseudo-landmarks are automatically
672 extracted from the root systems. Shortly, the image is divided vertically at equidistant posi-
673 tions (with the number defined by the user) and for each of the image stripes, the minimum
674 and maximum x coordinates are computed. The shape analysis is therefore able to discrim-
675 inate root system with different vertical root distributions or global root system orientation
676 (e.g. chemotropism) . The code source for the plugin, manual and sample images can be
677 found in the [github repository](#) of the project.

678 Statistical analysis was performed in R⁴⁵. The tidyR⁴⁶, dplyr⁴⁶, gridExtra⁴⁷, shapes⁴⁸,
679 geomorph⁴⁹ and ggplot2⁵⁰ packages were used for data preparation, analysis and plotting.
680 Final figure preparation was done in [Inkscape](#).

681 **Data availability** All the scripts and original data used to analyze and produce the images
682 can be accessed in the Github repository of the project: github.com/rr-lab/glo_roots. Raw
683 files of all the images used in the paper are availabe in [Dryad](#).

684 Acknowledgements

685 Work in the lab of JRD was funded by the Carnegie Institution for Science Endowment
686 and grants from the National Science Foundation (MCB-115795) and Department of En-
687 ergy, Biological and Environmental Research program (DE-SC0008769). RRA was sup-
688 ported by a Carnegie Postdoc Fellowship and currently by Conacyt Ciencia Básica Joven

689 Investigador grant number (CB-2014-01-238101). GL was supported by the Belgian Fonds
690 de la Recherche Scientifique. JM was funded by the National Science Foundation (IOS-
691 0820854). CH is funded by MGH Toteston & Fund for Medical Discovery Fellowship grant
692 2014A051303 and NIH R37 grant GM48707 and NSF grant MCB-0519898 awarded to Fred-
693 erick Ausubel, and previously by the Gordon and Betty Moore Foundation through Grant
694 GBMF 2550.01 from the Life Sciences Research Foundation. JV was funded by the Office
695 of Biological and Environmental Research, Office of Science, US Department of Energy, in-
696 teragency agreements DE-SC0001526 and DE-AI02-07ER64452. We thank Robert Mittler
697 and Philip Benfey for providing seeds of ZAT12:LUC and DR5:LUC+ respectively. We also
698 thank Neil Robbins for critical review of the manuscript an suggestions during the devel-
699 opment of the project. We greatly appreciate Tim Doyle's advice and help with luciferase
700 imaging.

701 **Competing interests**

702 We do not have any competing interests that we are aware of.

703 **Tables**

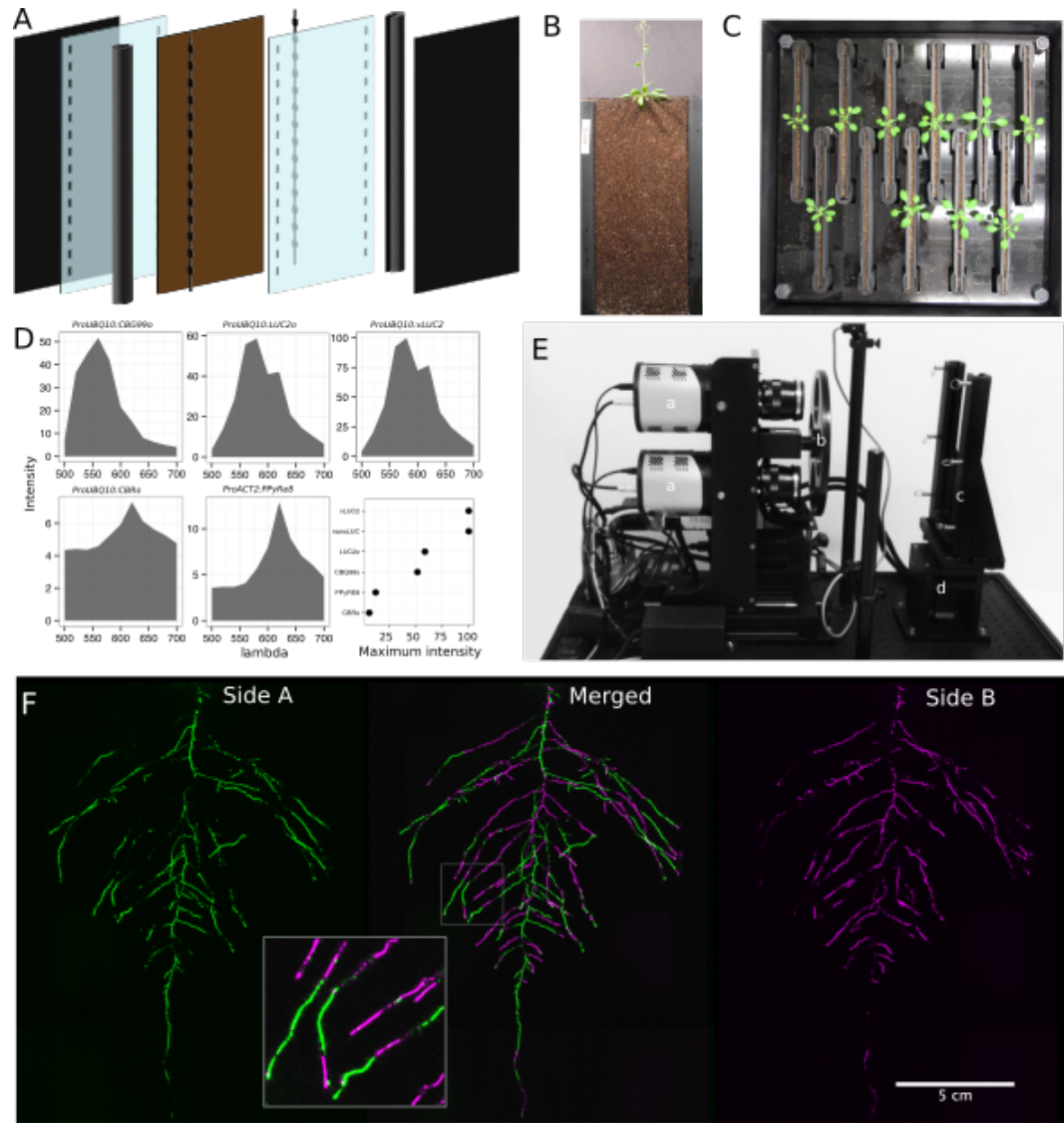
704 **Table 1:** Luciferases used in this study.

Luciferase	Origin	maximum wavelength	Substrate
Ppy RE8	firefly	618	D-luciferin
CBGRed	click beetle	615	D-luciferin
venus-LUC2	FP + firefly	580	D-luciferin
LUC(+)	firefly	578	D-luciferin
CBG99	click beetle	537	D-luciferin
lux operon	A. fischeri	490	biosynthesis pathway encoded within operon
nanoLUC	Deep sea shrimp	470	firimazine

705 **Table 2:** list of root system features extracted using GLO-RIA.

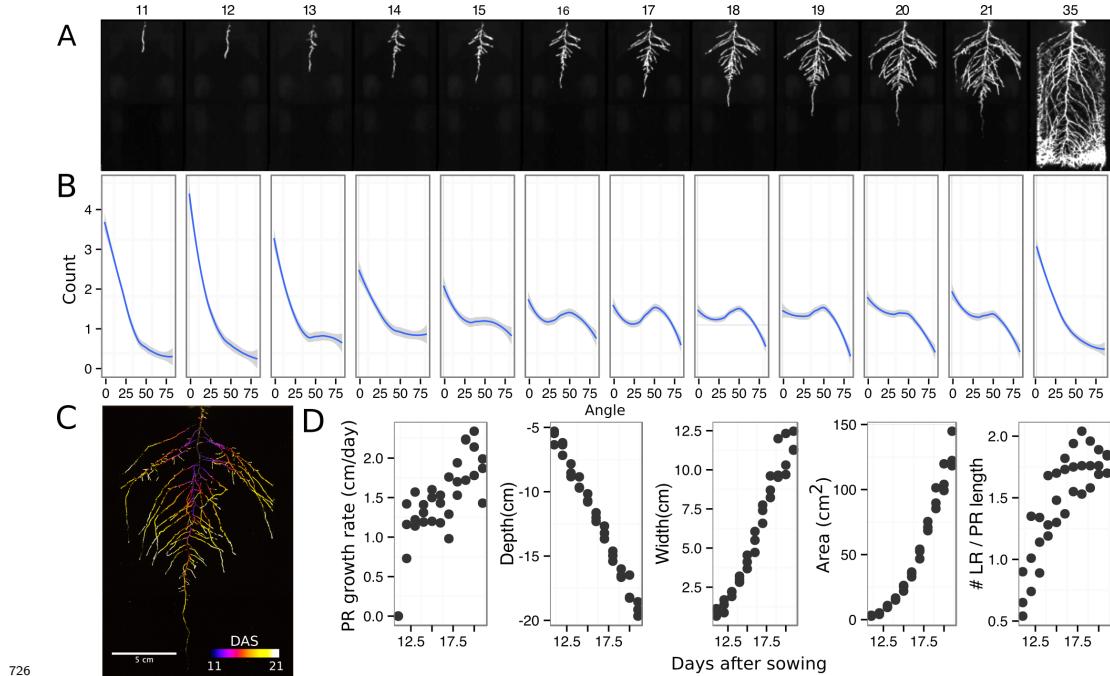
variable	unit
projected area	cm ²
number of visible roots	-
depth	cm
width	cm
convex hull area	cm ²
width	cm
feret	cm
feret angle	°
circularity	-
roundness	-
solidity	-
center of mass	cm
Directionality	°
Euclidean Fourier Descriptors	-
Pseudo landmarks	-

706 **Figures**



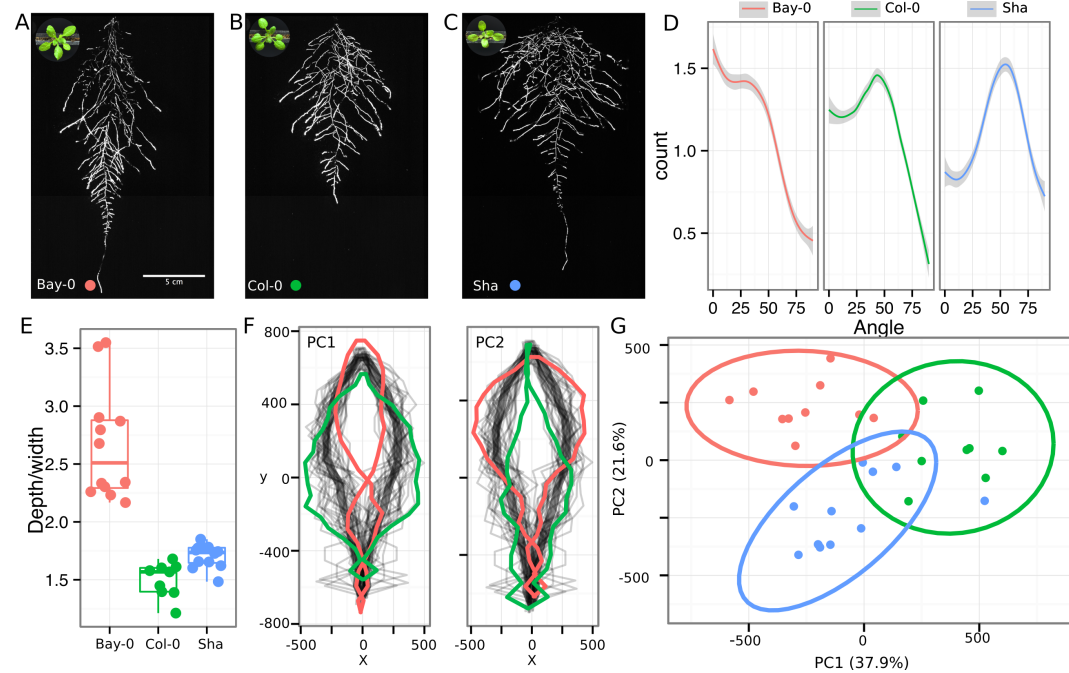
707
 708 **Figure 1.** A) 3D representation of the different components of the rhizotron: plastic
 709 covers, polycarbonate sheets, spacers and rubber U-channels. Blueprints are provided in
 710 Supplementary material 1. In brown, soil layer. B) Thirty five days old plant in rhizotron
 711 with black covers removed. C) Top view of holding box with eleven rhizotrons. D) In vivo
 712 emission spectra of different luciferases used in this study. Transgenic homozygous lines
 713 expressing the indicated transgenes were grown on agar media for 8 days. Luciferin (300

714 μM) was sprayed on the seedlings and plates were kept in the dark and then imaged for 2 s
 715 at wavelengths ranging from 500 to 700 nm. Five intensity values were taken from different
 716 parts of the roots of different seedlings and averaged. Relative maximum intensity values
 717 are indicated in the lower right graph. E) GLO 1 imaging system. The system is composed
 718 by two back illuminated CCD cameras (a) cooled down to -55°C . A filter wheel (b) allows
 719 for spectral separation of the different luciferases. On the right, a rhizotron holder (c) is
 720 used to position the rhizotrons in front of the cameras. A stepper motor (d) rotates the
 721 rhizotron 180° to image both sides. F) A 21 DAS plant expressing *ProUBQ10:LUC2o* was
 722 imaged on each of two sides of the rhizotron; luminescence signal is colorized in green or
 723 magenta to indicate side. In the middle of the panel, a combined image of the two sides
 724 is shown. The inset shows a magnified part of the root system. FW: fresh weight, PR:
 725 Primary root.



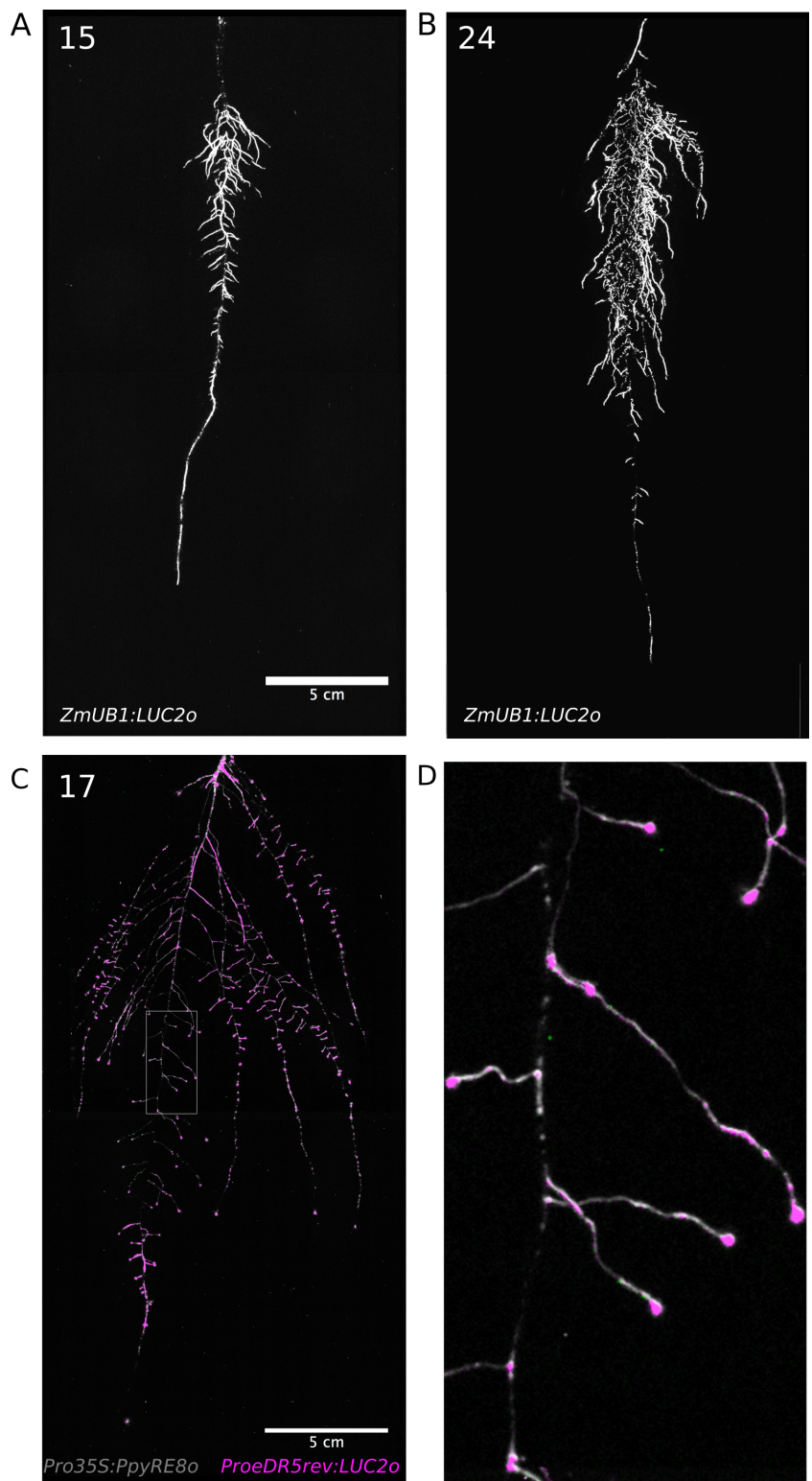
726 **Figure 2:** A) Typical daily time-lapse image series from 11 to 21 DAS of a
 727 *ProUBQ10:LUC2o* Col-0 plant. B) Directionality of the root system of plants in
 728 panel A calculated using the directionality plugin implemented in GLO-RIA. C) Color
 729 coded projection of root growth using the images in panel A. D) Primary root growth
 730 parameters.

731 rate, depth, width, root system area are automatically calculated from the convex hull,
 732 which is semi-automatically determined with GLO-RIA. Lateral root number and number
 733 of lateral roots divided by the primary root length were quantified manually. A Local
 734 Polynomial Regression Fitting with 95% confidence interval (grey) was used to represent
 735 the directionality distribution curve. (0° is the direction of the gravity vector).



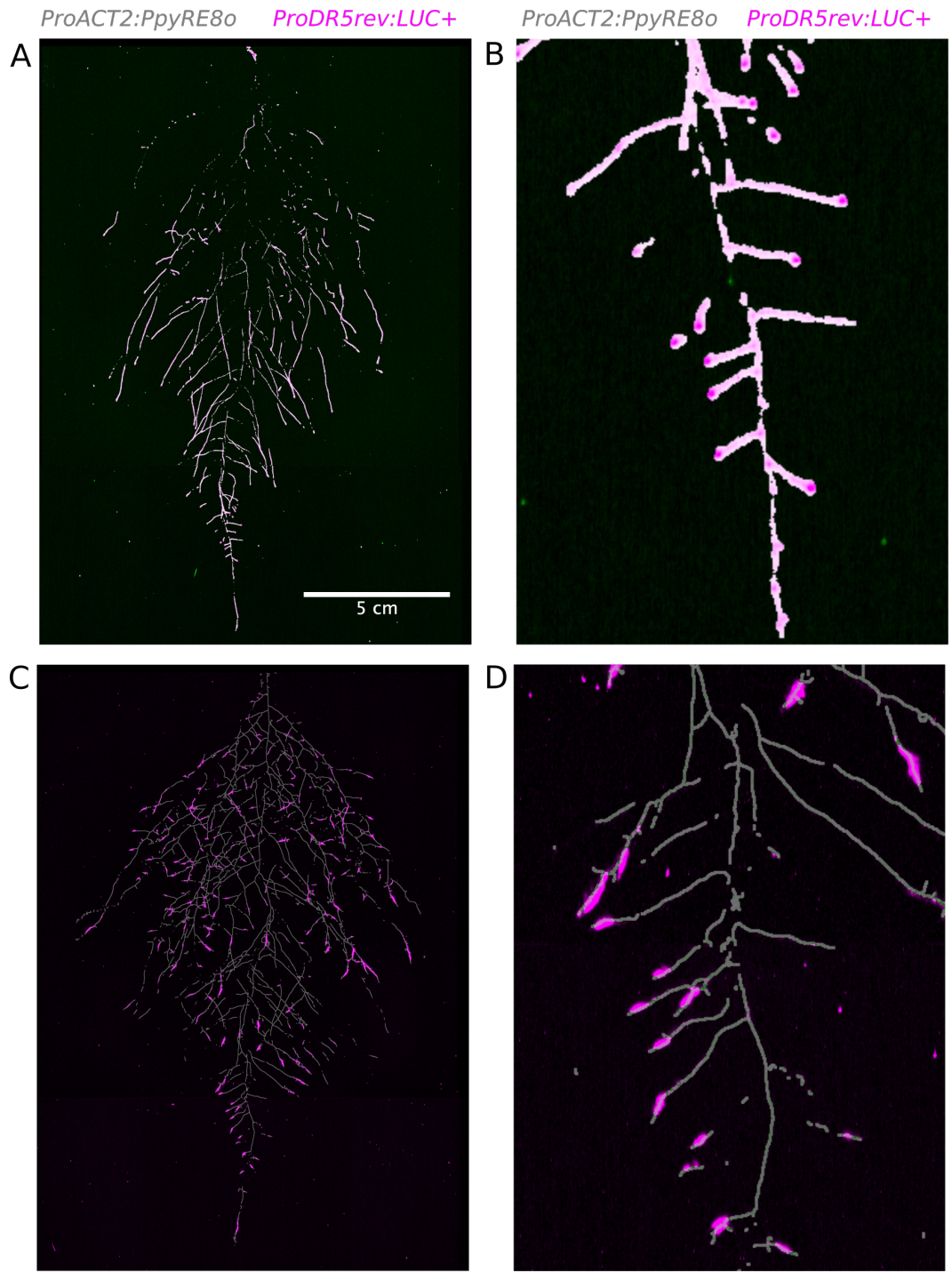
737 **Figure 3.** Representative root and shoot images of A) Bay-0, B) Col-0 and C) Sha acce-
 738 sions 22 DAS transformed with *ProUBQ10:LUC2o*. D) Directionality of the root systems, E)
 739 depth/width ratio, F) Elliptic Fourier Descriptors of shape variation in root system architec-
 740 ture. Eigenvalues derived from the analysis of 9-12 plants per accession is shown. The first
 741 two Principal Components explaining 38% (PC1) and 22% (PC2) of the shape variation are
 742 plotted. PC1 captures homogeneity of root system width along the vertical axis with and
 743 PC2 a combination of depth and width in top parts of the root sytem. Red and green lines
 744 indicate -3SD and +3SD, respectively G) PCA separation of the different ecotypes using
 745 the PC described in F. A Local Polynomial Regression Fitting with 95% confidence interval
 746 (grey) was used to represent the directionality distribution curve. (0° is the direction of the
 747 gravity vector). Wilcoxon test analysis with $p < 0.01$ was used to test significant differences

⁷⁴⁸ between the different accession (n = 9-12 plants).



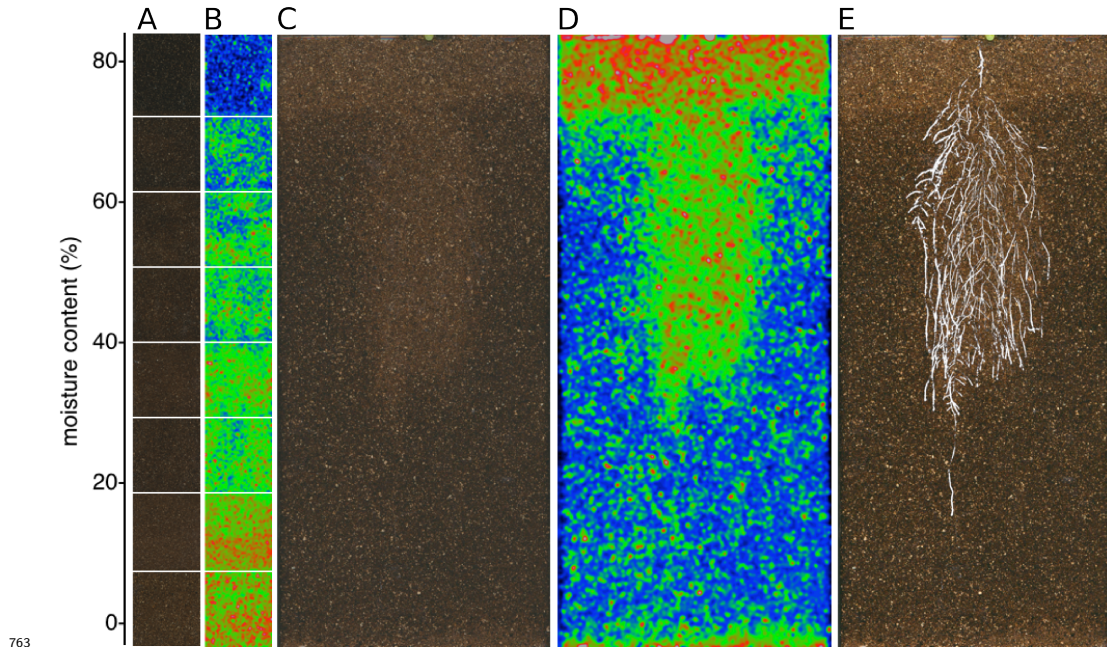
749

750 **Figure 4:** Roots of *Brachypodium distachyon* transformed with *ProZmUB1:LUC2o* and
751 imaged at 15 (A) and 24 (B) DAS grown in control conditions. C) 17 DAS tomato plant
752 transformed with *ProeDR5rev:LUC2o* (magenta) and *Pro35S:PPyRE8o* (grey) D) Zoomed
753 inset of root in panel D showing increased expression of *ProeDR5rev:LUC2o* reporter in
754 early-stage lateral roots.

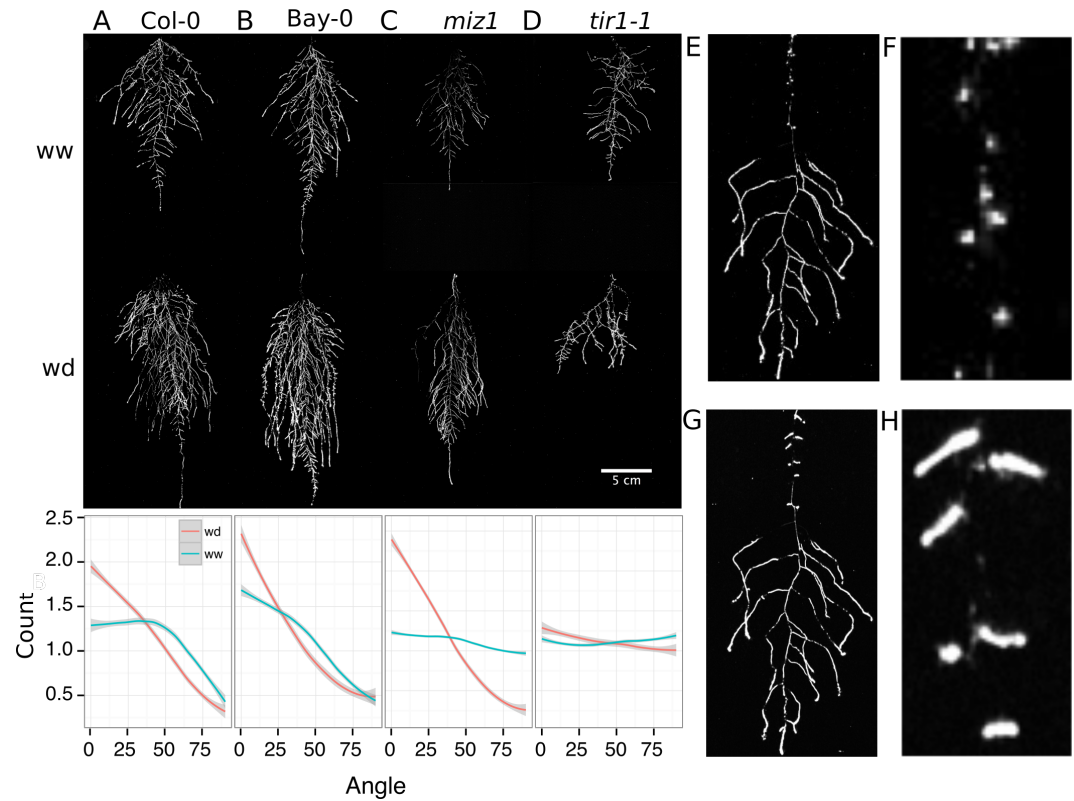


756 **Figure 5:** Images of whole root systems (A, C) or magnified portion of roots (B, D) at 22
757 DAS expressing *ProDR5rev:LUC+* (magenta, A, B) or *ProZAT12:LUC* signal (magenta,

758 C, D)with skeletonized representation of roots generated using the *ProACT2:PpyRE80*
759 reporter expression (in grey). E) Visualization of the results obtained by analyzing the
760 ZAT12:LUC image with the GLO-RIA Root Reporter module. Blue circles are proportional
761 in size to the ZAT12:LUC intensity value. Hovering over the points will reveal numerical
762 values for the ZAT12:LUC intensity

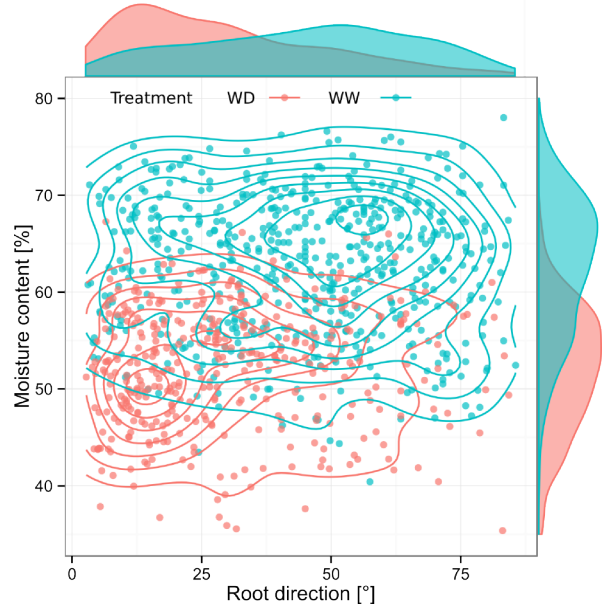


764 **Figure 6:** Soil moisture mapping in rhizotrons. A) Composite image strip made from
765 rhizotrons prepared with different soil moisture levels. B) Differences in grey-scale intensity
766 values were enhanced using a 16-color Look Up Table (LUT). Brightfield image of soil in
767 rhizotron (C) and converted using 16-color LUT to enhance visualization of distribution of
768 moisture (D) . E) Root system of a Bay-0 22 DAS and subjected to water deprivation since
769 13 DAS. Root system visualized using luminescence and overlaid on brightfield image of soil
770 in (C).



771

772 **Figure 7:** A-D) Root systems 22 DAS and exposed to water deficit 13 DAS onwards.
 773 Sample images of well watered (left panels) and water deficit (right panels) root systems
 774 started 13 DAS and directionality (line graphs to left of images) for (A) Col-0 (B) Bay-0
 775 (C) *miz1* mutant and (D) *tir1-1*. E) Root system of a 22 DAS plant exposed to water
 776 deprivation from 9 DAS onwards with magnified view of lateral root primordia (F). G) The
 777 same root as in (E) 24 hours after rewatering and magnified view of lateral root primordia
 778 (H). Kolmogorov-Smirnov test at $p < 0.001$ was used to compare directionality distributions
 779 between the different treatments and genotypes. A Local Polynomial Regression Fitting
 780 with 95% confidence interval (grey) was used to represent the directionality distribution
 781 curve. (0° is the direction of the gravity vector).



782 **Figure 8:** Relationship between local soil moisture content and root growth direction. Data
 783 quantified from the time lapse shown in [Video 3](#). Density plots shown at periphery of graph
 784 for root direction (x-axis) and soil moisture (y-axis). (0° is the direction of the gravity
 785 vector).
 786

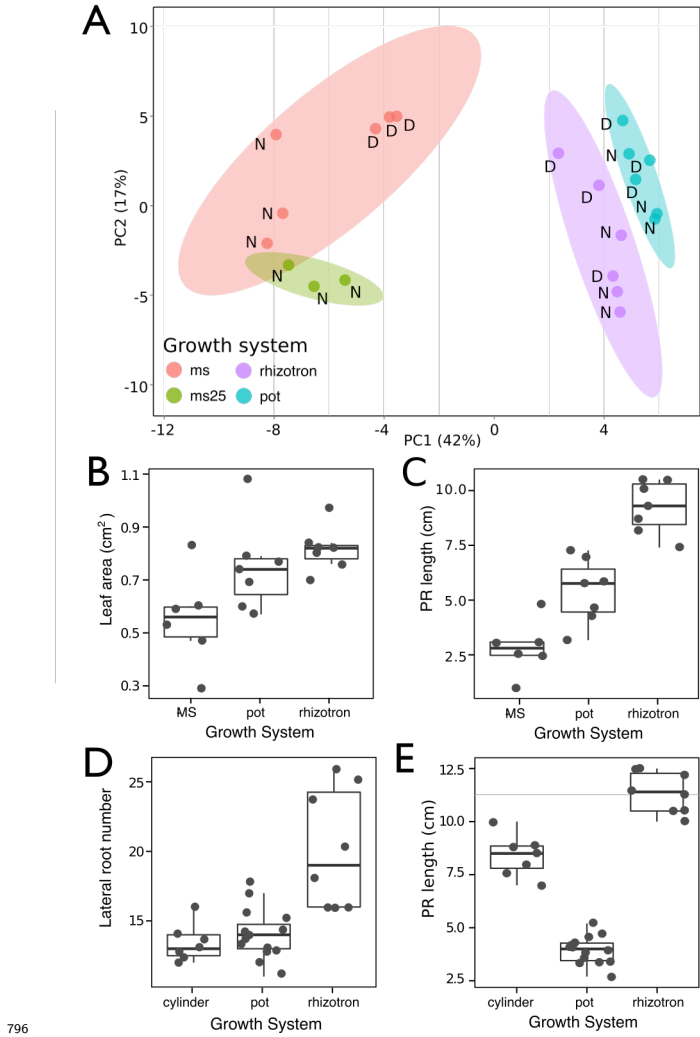
787 Videos

788 [Video 1](#) Time lapse from 11 to 21 DAS of a Col-0 plant expressing *ProUBQ10:LUC2o*
 789 grown in control conditions

790 [Video 2](#) 24 h time lapse a Col-0 plant expressing *ProACT2:PpyRE8* (gray) and *ZAT12:LUC*
 791 (magenta) after addition of a 1 M solution of NaCl on the right side of the plant.

792 [Video 3](#) Time lapse from 16 to 24 DAS of Col-0 plants expressing *ProUBQ10:LUC2o*
 793 growing in water deficient conditions (left) and control (right). Plants were sown under
 794 control conditions and water deficit treatment started 11 DAS.

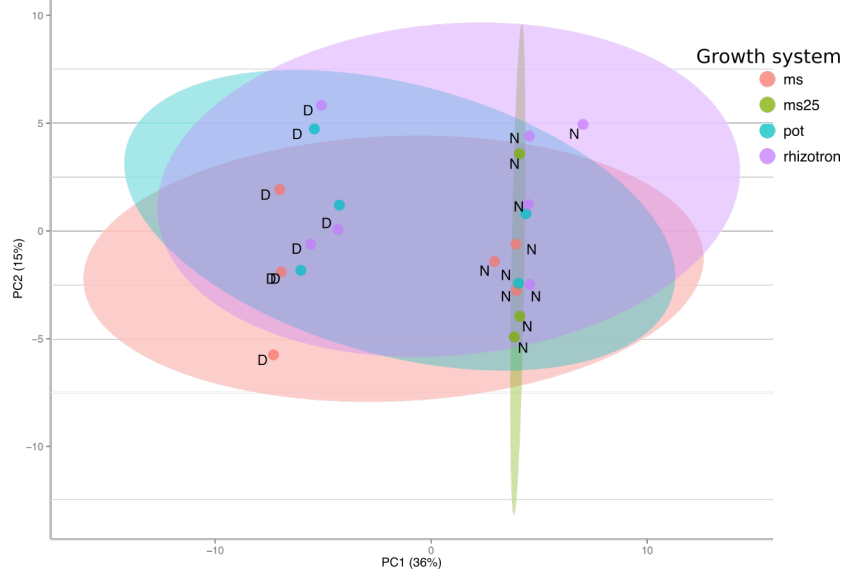
795 **Supplementary Material**



796

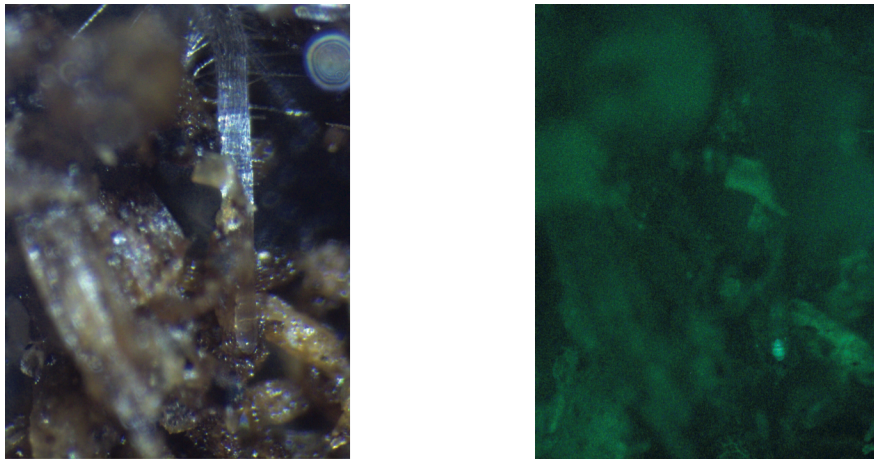
797 **Figure 1-figure supplement 1** A) Principal Components Analysis (PCA) score plot of
 798 a set of 77 genes analyzed by qPCR from root samples of plants grown in MS plates, pots,
 799 and rhizotrons. After 15 DAS three plants were collected at the end of the day (D) and
 800 three were collected at the end of the night (N). (ms = plant grown in full ms, ms25 =
 801 plants grown in 25% of full ms) B) Lateral root number and G) primary root length of 18
 802 DAS plants grown in 30 cm tall cylinders, pots and rhizotrons, all with a volume of 100 cm^3
 803 ($n = 6-12$ plants). D) Leaf area and E) primary root length of plants of the same age (15
 804 DAS) as the ones used for the qPCR experiment ($n= 6-7$). ANOVA analysis with $p < 0.01$

805 was used to test significant differences between the different parameters.

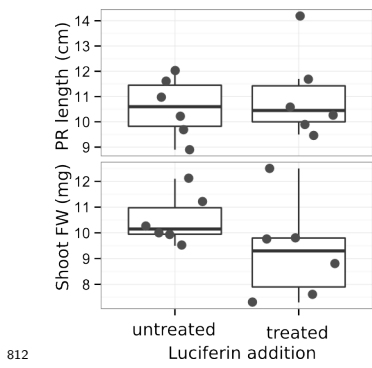


806
807 **Figure 1-figure supplement 2** PCA plot of shoots of the same samples used in Figure 1.

808 See Figure 1 for more details regarding experimental conditions used.

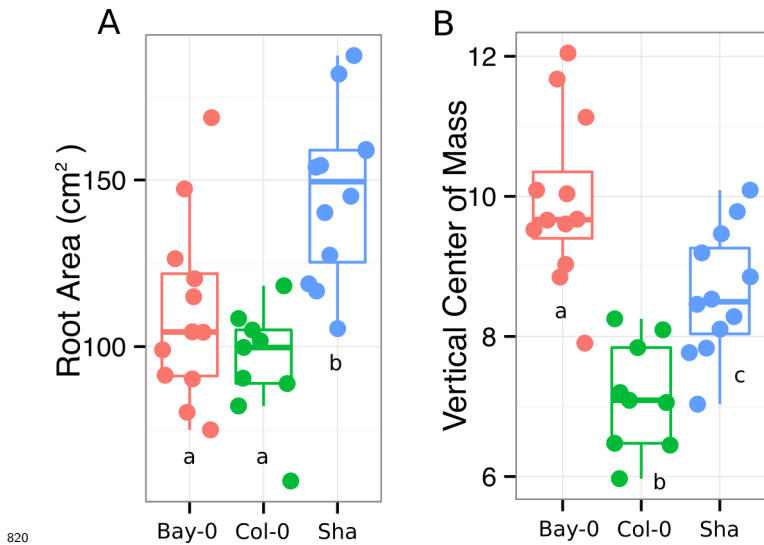


809
810 **Figure 1-figure supplement 3** Image of a an Arabidopsis root in soil under with white
811 light (brightfield) and GFP excitation light.

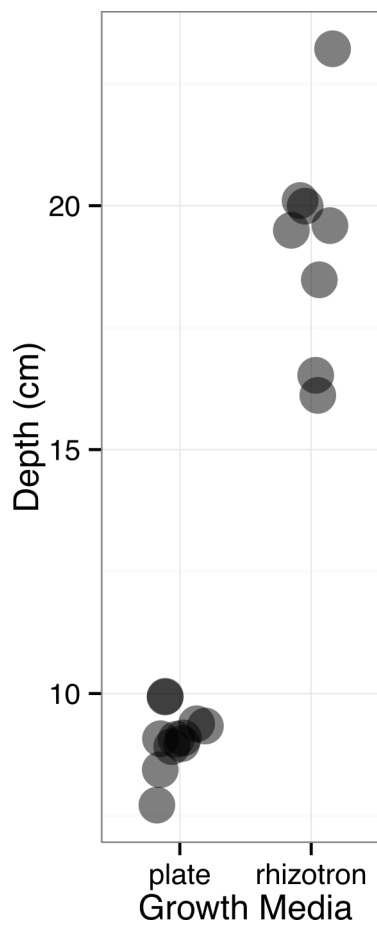


812
813 **Figure 1-figure supplement 4** Effect of luciferin addition on the primary root length and
814 shoot size of 14 DAS seedlings that were either continuously exposed to 300 μ M luciferin
815 from 9 DAS after sowing or not.

816 **Figure 1-figure supplement_data_1:** Two way ANOVA P-values comparing plants
817 grown in MS media vs plants grown in soil (pots or rhizotrons) and plants collected at day
818 or night. We used p-value < 0.00065 threshold based on Bonferroni adjustment for multiple
819 testing.

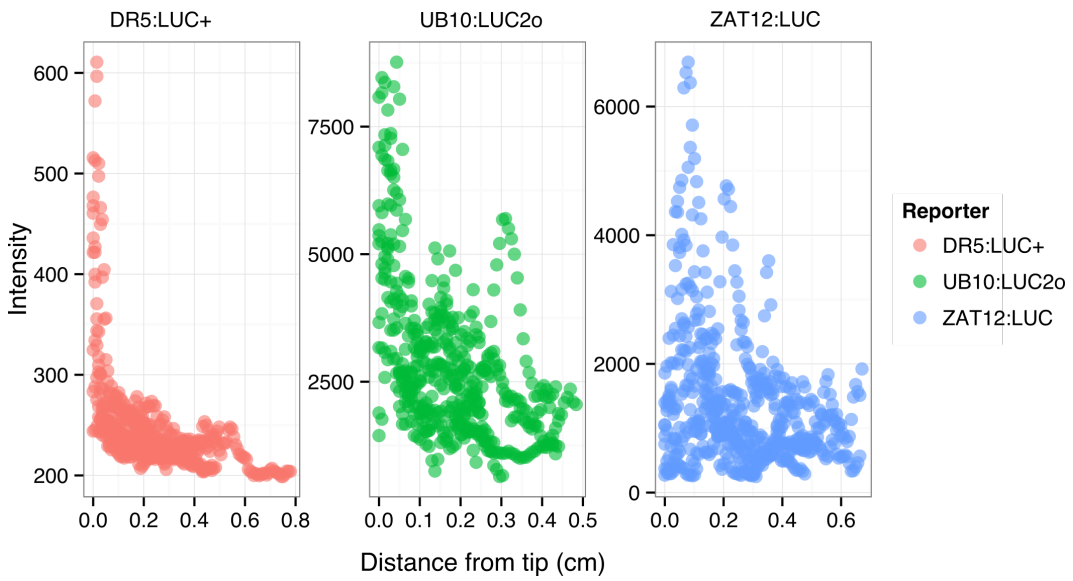


820
821 **Figure 3-figure supplement 1** A) root area, B) vertical center of mass of Bay-0, Col-0
822 and Sha accessions.



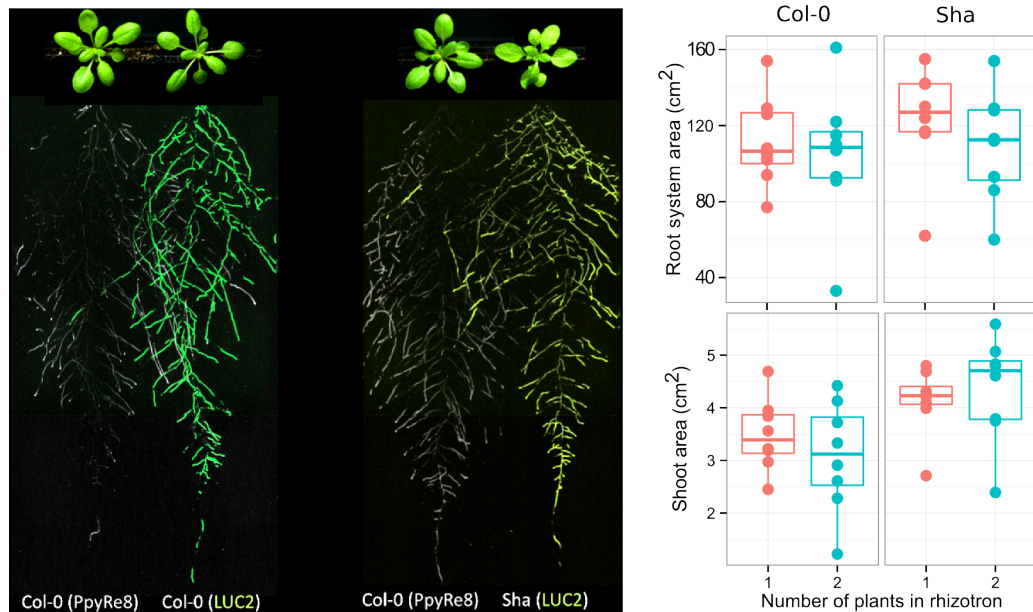
823

824 **Figure 4-figure supplement 1** Depth of the primary root of *Brachypodium* plants grown
825 in rhizotrons or on gel-based media (n=8-11).



826

827 **Figure 5-figure supplement 1** Dual color images of 22 DAS plants growing in the
 828 same rhizotron and expressing different luciferases. A) Two Col-0 plants expressing
 829 *ProUBQ10:LUC2o* and *ProACT2:PPyRE8o* B) Col-0 plant expressing *ProACT2:PPyRE8o*
 830 and Sha plant expressing *ProUBQ10:LUC2o*.



832 **Figure 5-figure supplement 2:** A) Triple color picture showing a 22 DAS
 833 *ProUBQ10:LUC2o* plant (magenta) grown in the same rhizotron with *ProACT2:PPyRE8o*

834 plants (grey). Plants were inoculated with *Pseudomonas fluorescens* CH267 (green)
835 Magnified portion of root systems colonized by *Pseudomonas fluorescens* showing *P.*
836 *fluorescences* (B) only or all three reporters together (C).

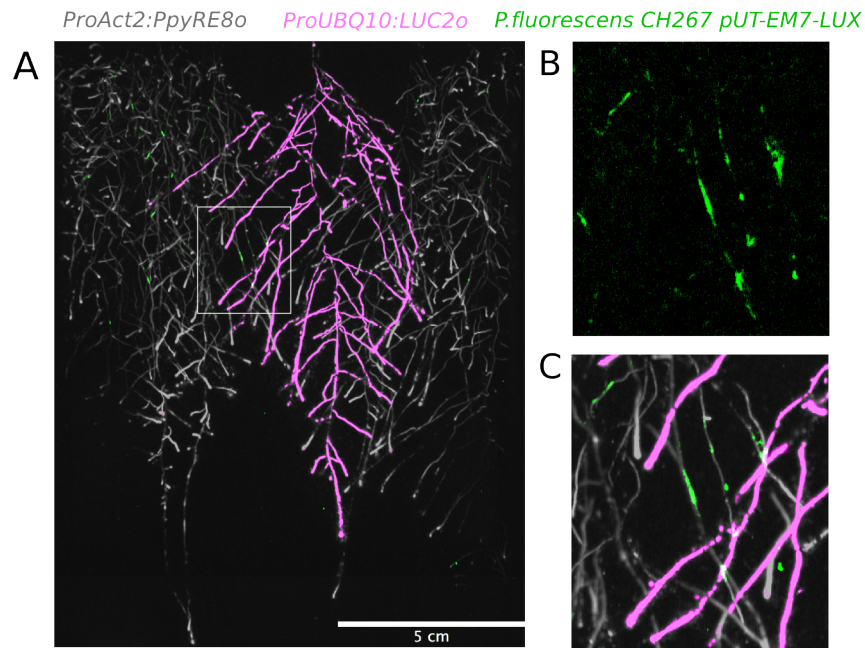
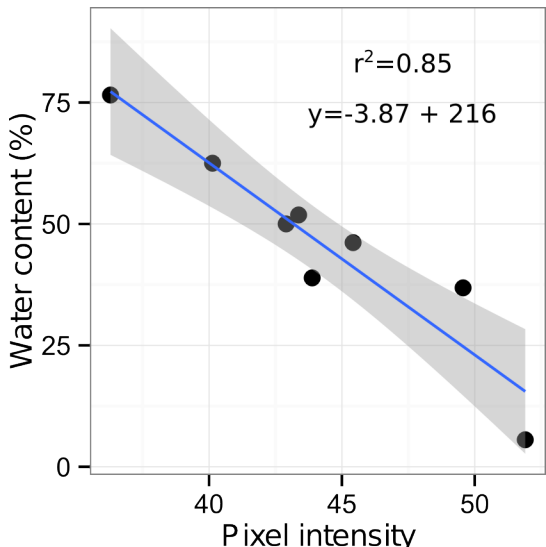


Figure 5-figure

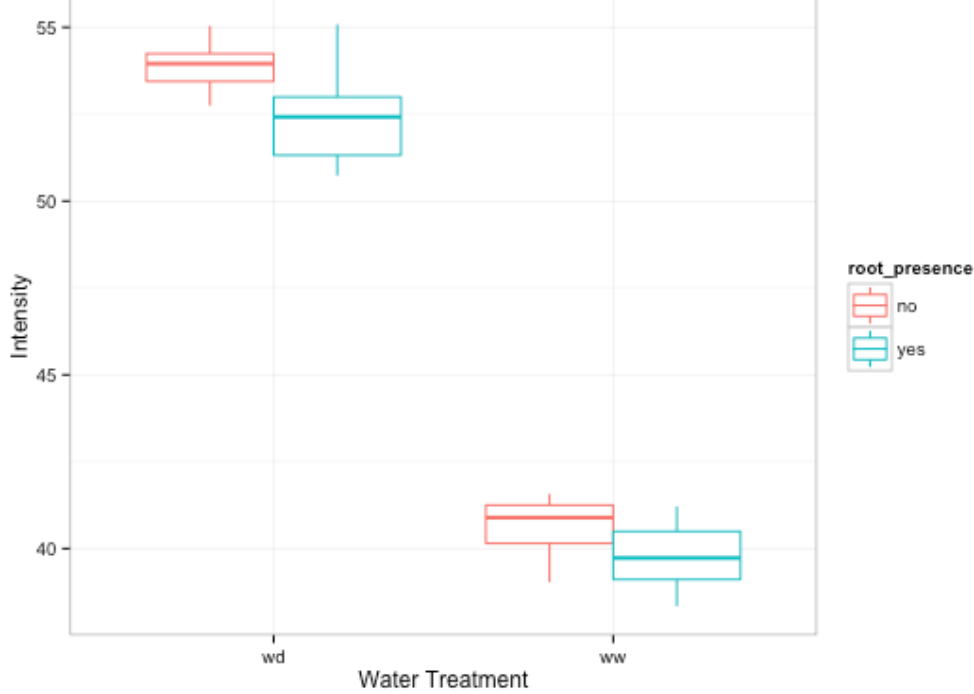
838 **supplement 3:** DR5:LUC+, UBQ10:LUC2o and ZAT12:LUC intensity values along the
839 root tip. Data was manually obtained by obtaining the intensity profile of the first 0.3-0.8
840 cm from the root tip of individual lateral roots. Ten lateral roots for each reporter were
841 measured.



842

Figure 6-figure supplement 1: Moisture

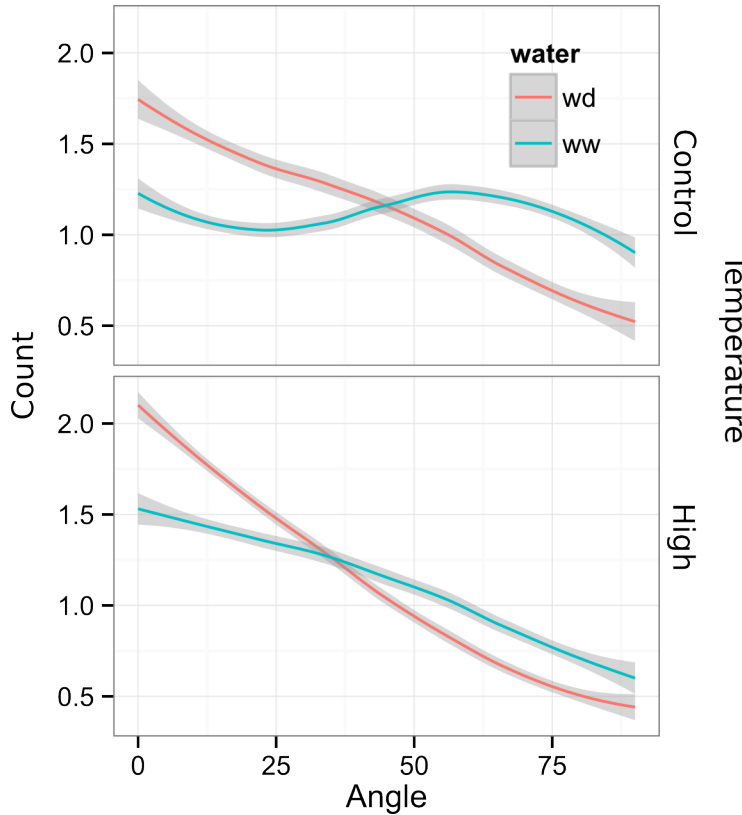
843 calibration curve. Rhizotrons with different levels of moisture were prepared and scanned
 844 to obtain readings of pixel intensity. Soil from rhizotrons was then weighed, dried down in
 845 an oven at 70 °C for 48 hours and percent water content quantified.



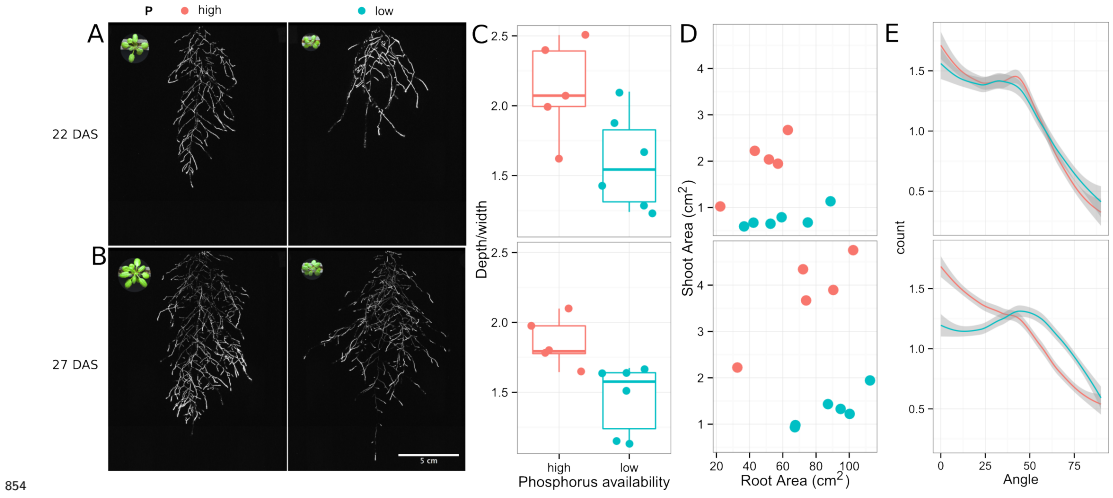
846

847 **Figure 6-figure supplement 2:** Comparison of soil intensity values between areas of the

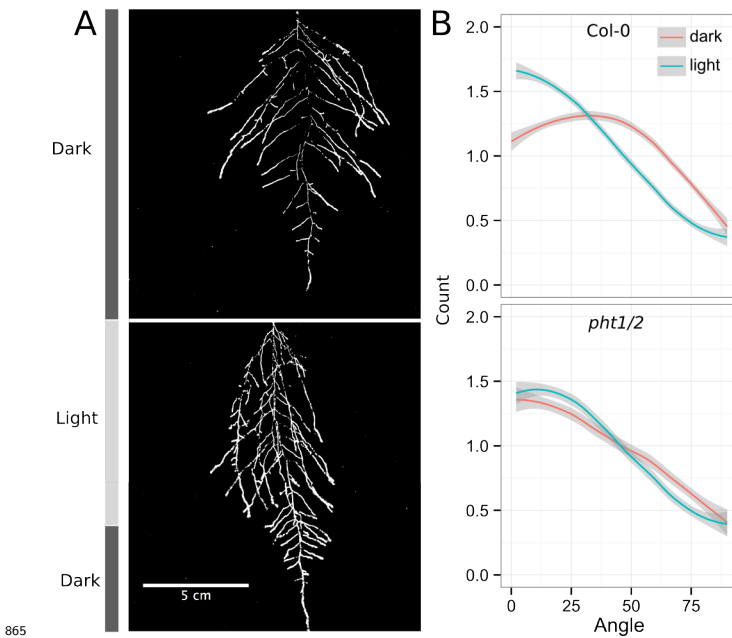
848 rhizotron with or without root presence. Mean intensity values from 100 x 100 pixel squares
849 samples of both areas were obtained from 10 different rhizotrons.



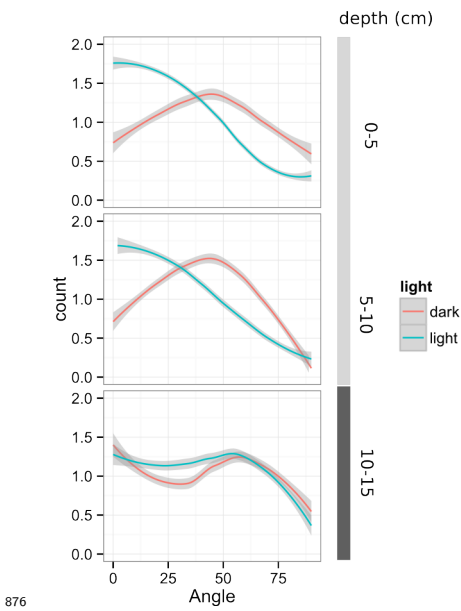
850
851 **Figure 7-figure supplement 1** Directionality analysis of roots of plants transferred to
852 water deprivation conditions after 9 DAS and kept 22 °C (control temperature) and 29 °C
853 (high temperature) until 22 DAS. (0° is the direction of the gravity vector).



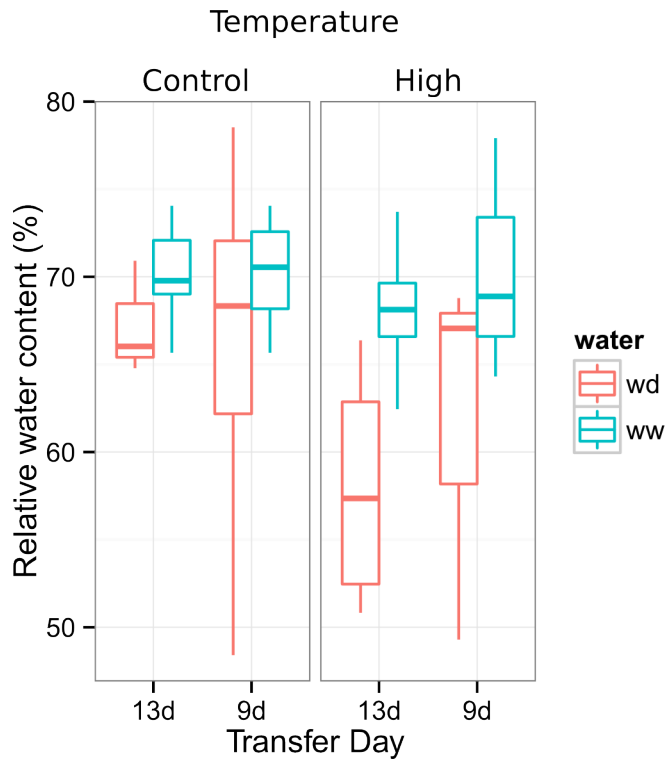
854 **Figure 7-figure supplement 2** Shoot and root systems of *ProUBQ10:LUC2o* Col-0
 855 plants growing in soil supplemented with 1ml of 100 μM P-Alumina (left) and 0-P-Alumina
 856 (right) 22 (A) or 27 (B) DAS. C) Root depth/width ratio of 22 (top) and 27 (bottom)
 857 DAS plants. D) Scatter-plot showing relationship between root and shoot system area at
 858 22 (top) and 27 (bottom) DAS. E) Root directionality distribution in plants 22 (top) and
 859 27 (bottom) DAS. Anova analysis at $p < 0.01$ was used to compare depth/width ratios in
 860 P treatments. Kolmogorov-Smirnov test at $p < 0.001$ was used to compare directionality
 861 distributions between the different treatments. A Local Polynomial Regression Fitting
 862 with 95% confidence interval (grey) was used to represent the directionality distribution
 863 curve. (0° is the direction of the gravity vector).



865 **Figure 7-figure supplement 3** A) Col-0 root systems shielded (top) or light exposed
 866 (bottom). After 9 DAS the top third of the rhizotron was exposed to light (indicated
 867 on the side with a light grey bar) and plants were imaged at 20 DAS. B) Directionality
 868 analysis of root systems shielded (red) or exposed (green) to light for Col-0 (top panel)
 869 or *pht1/2* double mutant (bottom panel). Between 4 and 6 plants were analyzed per
 870 treatment. ANOVA analysis at $p < 0.01$ was used to compare depth/width ratios in P
 871 treatments. Kolmogorov-Smirnov test at $p < 0.001$ was used to compare directionality
 872 distributions between the different treatments. A Local Polynomial Regression Fitting with
 873 95% confidence interval (grey) was used to represent the directionality distribution curve. (0°
 874 is the direction of the gravity vector).



877 **Figure 7-figure supplement 4** Plots showing output of directionality analysis performed
 878 at different depths (0-5, 5-10, 10-15 cm) in rhizotrons exposed to light or kept in the dark.
 879 (0° is the direction of the gravity vector).



881 **Figure 7-figure supplement 5** Leaf relative water content of 23 DAS plants that were
882 subjected to water deprivation (ww) after 9 or 13 DAS or kept under well watered (ww)
883 conditions. At 9 DAS half of the plants were kept under control temperature conditions (22
884 °C) and the other half transferred to a 29 °C (high) chamber. n = 6-8 plants.

885 **Supplemental Material 1**

886 Blueprints of the holders, clear sheets and spacers needed to built the rhizotrons. Additional
887 details are provided in the materials and methods. Files are provided in Adobe Illustrator
888 .ai and Autocad .dxf formats.

889 **Supplemental Material 2**

890 Primers used in the qPCR experiment.

891 **Supplemental Material 3**

892 Vector maps of all the constructs used in this work.

893 **References**

- 894 1.Dinneny, J. R. *et al.* Cell identity mediates the response of *Arabidopsis* roots to abiotic
895 stress. *Science* **320**, 942–945 (2008).
- 896 2.Duan, L. *et al.* Endodermal ABA Signaling Promotes Lateral Root Quiescence during
897 Salt Stress in Arabidopsis Seedlings. *Plant Cell* **25**, 324–341 (2013).
- 898 3.Lynch, J. P. & Wojciechowski, T. Opportunities and challenges in the subsoil: pathways
899 to deeper rooted crops. *J. Exp. Bot.* **66**, 2199–2210 (2015).
- 900 4.Brady, N. C. & Weil, R. R. *Elements of the nature and properties of soils*. (Prentice Hall,
901 2009).
- 902 5.Bao, Y. *et al.* Plant roots use a patterning mechanism to position lateral root branches
903 toward available water. *Proc Natl Acad Sci* **111**, 9319–9324 (2014).
- 904 6.Tabata, R. *et al.* Perception of root-derived peptides by shoot LRR-RKs mediates systemic
905 N-demand signaling. *Science* **346**, 343–346 (2014).

- 906 7.Rosquete, M. R. *et al.* An Auxin Transport Mechanism Restricts Positive Orthogravit-
907 ropism in Lateral Roots. *Current Biology* **23**, 817–822 (2013).
- 908 8.Uga, Y. *et al.* Control of root system architecture by DEEPER ROOTING 1 increases
909 rice yield under drought conditions. *Nat. Genet.* **45**, 1097–1102 (2013).
- 910 9.Postma, J. A. & Lynch, J. P. The optimal lateral root branching density for maize depends
911 on nitrogen and phosphorus availability. *Plant Physiol.* **166**, 590–602 (2014).
- 912 10.Schneider, C. A., Rasband, W. S. & Eliceiri, K. W. NIH Image to ImageJ: 25 years of
913 image analysis. *Nature methods* **9**, 671–675 (2012).
- 914 11.Hara-Miyauchi, C. *et al.* Bioluminescent system for dynamic imaging of cell and animal
915 behavior. *Biochem. Biophys. Res. Commun.* **419**, 188–193 (2012).
- 916 12.Emami, S., Yee, M.-C. & Dinneny, J. R. A robust family of Golden Gate Agrobacterium
917 vectors for plant synthetic biology. *Front. Plant Sc.* **4**, 339 (2013).
- 918 13.Ristova, D. *et al.* RootScape: a landmark-based system for rapid screening of root
919 architecture in Arabidopsis. *Plant Physiology* **161**, 1086–1096 (2013).
- 920 14.Lobet, G. *et al.* Root System Markup Language: toward a unified root architecture
921 description language. *Plant Physiol.* **167**, 617–627 (2015).
- 922 15.Meijon, M., Satbhai, S. B., Tsuchimatsu, T. & Busch, W. Genome-wide association study
923 using cellular traits identifies a new regulator of root development in. *Nat. Genet.* **46**, 77–81
924 (2013).
- 925 16.Pacheco-Villalobos, D. & Hardtke, C. S. Natural genetic variation of root system archi-
926 tecture from Arabidopsis to Brachypodium: towards adaptive value. *Philosophical Trans-
927 actions of the Royal Society of London B: Biological Sciences* **367**, 1552–1558 (2012).
- 928 17.Watt, M., Schneebeli, K., Dong, P. & Wilson, I. W. The shoot and root growth of
929 Brachypodium and its potential as a model for wheat and other cereal crops. *Functional
930 Plant Biol.* **36**, 960–969 (2009).
- 931 18.Mann, D. G. J. *et al.* Gateway-compatible vectors for high-throughput gene functional

- 932 analysis in switchgrass (*Panicum virgatum* L.) and other monocot species. *Plant Biotechnol.*
933 *J.* **10**, 226–236 (2012).
- 934 19.Pacheco-Villalobos, D., Sankar, M., Ljung, K. & Hardtke, C. S. Disturbed Local
935 Auxin Homeostasis Enhances Cellular Anisotropy and Reveals Alternative Wiring of
936 Auxin-ethylene Crosstalk in *Brachypodium distachyon* Seminal Roots. *PLoS Genet* **9**,
937 e1003564 (2013).
- 938 20.Buer, C. S., Wasteneys, G. O. & Masle, J. Ethylene modulates root-wave responses in
939 *Arabidopsis*. *Plant Physiology* **132**, 1085–1096 (2003).
- 940 21.Moreno-Risueno, M. A. *et al.* Oscillating gene expression determines competence for
941 periodic *Arabidopsis* root branching. *Science* **329**, 1306–1311 (2010).
- 942 22.Miller, G. *et al.* The plant NADPH oxidase RBOHD mediates rapid systemic signaling
943 in response to diverse stimuli. *Science Signaling* **2**, ra45 (2009).
- 944 23.Haney, C. H., Samuel, B. S., Bush, J. & Ausubel, F. M. Associations with rhizo-
945 sphere bacteria can confer an adaptive advantage to plants. *Nature Plants* 15051 (2015).
946 doi:[10.1038/nplants.2015.51](https://doi.org/10.1038/nplants.2015.51)
- 947 24.Mandoli, D. F., FORD, G. A., WALDRON, L. J., NEMSON, J. A. & Briggs, W. R. Some
948 spectral properties of several soil types: implications for photomorphogenesis*. *Plant Cell*
949 *Environ.* **13**, 287–294 (1990).
- 950 25.Galen, C., Rabenold, J. J. & Liscum, E. Functional ecology of a blue light photoreceptor:
951 effects of phototropin-1 on root growth enhance drought tolerance in *Arabidopsis thaliana*.
952 *New Phytol.* **173**, 91–99 (2007).
- 953 26.Moni, A., Lee, A. Y., Briggs, W. R. & Han, I. S. The blue light receptor Phototropin 1
954 suppresses lateral root growth by controlling cell elongation. *Plant Biology* 34–40 (2014).
- 955 27.Yokawa, K., Kagenishi, T. & Baluška, F. Root photomorphogenesis in laboratory-
956 maintained *Arabidopsis* seedlings. *Trends Plant Sci.* **18**, 117–119 (2013).
- 957 28.Lobell, D. B. *et al.* Greater Sensitivity to Drought Accompanies Maize Yield Increase in

- 958 the U.S. Midwest. *Science* **344**, 516–519 (2014).
- 959 29.Ort, D. R. & Long, S. P. Limits on Yields in the Corn Belt. *Science* **344**, 484–485 (2014).
- 960 30.Blossfeld, S., Schreiber, C. M., Liebsch, G., Kuhn, A. J. & Hinsinger, P. Quantitative
961 imaging of rhizosphere pH and CO₂ dynamics with planar optodes. *Annals of Botany* **112**,
962 267–276 (2013).
- 963 31.Shaw, S. L. & Ehrhardt, D. W. Smaller, Faster, Brighter: Advances in Optical Imaging
964 of Living Plant Cells. *Annu. Rev. Plant Biol.* **64**, 351–375 (2013).
- 965 32.Barr, H. & Weatherley, P. A re-examination of the relative turgidity technique for esti-
966 mating water deficit in leaves. *Aust. J. Biol. Sci* **15**, 413–428 (1962).
- 967 33.Grapov, D. DeviumWeb: Dynamic Multivariate Data Analysis and Visualization Plat-
968 form.
- 969 34.Branchini, B. R. *et al.* Red-emitting luciferases for bioluminescence reporter and imaging
970 applications. *Analytical Biochemistry* **396**, 290–297 (2010).
- 971 35.Branchini, B. R. *et al.* Thermostable red and green light-producing firefly luciferase
972 mutants for bioluminescent reporter applications. *Analytical Biochemistry* **361**, 253–262
973 (2007).
- 974 36.Hall, M. P. *et al.* Engineered Luciferase Reporter from a Deep Sea Shrimp Utilizing a
975 Novel Imidazopyrazinone Substrate. *ACS Chem. Biol.* **7**, 1848–1857 (2012).
- 976 37.Lane, M. C., Alteri, C. J., Smith, S. N. & Mobley, H. L. T. Expression of flagella is
977 coincident with uropathogenic Escherichia coli ascension to the upper urinary tract. *Proc.
978 Natl. Acad. Sci. U.S.A.* **104**, 16669–16674 (2007).
- 979 38.Ruegger, M. *et al.* The TIR1 protein of Arabidopsis functions in auxin response and is
980 related to human SKP2 and yeast grr1p. *Genes Dev* **12**, 198–207 (1998).
- 981 39.Moriwaki, T. *et al.* Hormonal Regulation of Lateral Root Development in Arabidopsis
982 Modulated by MIZ1 and Requirement of GNOM Activity for MIZ1 Function. *Plant Physiol.*
983 **157**, 1209–1220 (2011).

- 984 40.Vogel, J. & Hill, T. High-efficiency Agrobacterium-mediated transformation of Brachy-
985 podium distachyon inbred line Bd21-3. *Plant Cell Rep* **27**, 471–478 (2008).
- 986 41.Covington, M. F. & Harmer, S. L. The Circadian Clock Regulates Auxin Signaling and
987 Responses in Arabidopsis. *Plos Biol* **5**, e222 (2007).
- 988 42.Lindeboom, J. J. *et al.* A Mechanism for Reorientation of Cortical Microtubule Arrays
989 Driven by Microtubule Severing. *Science* **342**, 1245533–1–1245533–11 (2013).
- 990 43.Chitwood, D. H. *et al.* A modern ampelography: a genetic basis for leaf shape and
991 venation patterning in grape. *Plant Physiology* **164**, 259–272 (2014).
- 992 44.Iwata, H. & Ukai, Y. SHAPE: a computer program package for quantitative evaluation of
993 biological shapes based on elliptic Fourier descriptors. *The Journal of heredity* **93**, 384–385
994 (2002).
- 995 45.R Core Team. *R: A language and environment for statistical computing*. (R Foundation
996 for Statistical Computing, 2014). at <<http://www.R-project.org/>>
- 997 46.Wickham, H. *Tidyr: Easily tidy data with spread() and gather() functions*. (2014). at
998 <<http://CRAN.R-project.org/package=tidyr>>
- 999 47.Auguie, B. *GridExtra: Functions in grid graphics*. (2012). at <<http://CRAN.R-project.org/>>
- 1000 1001 48.Dryden, I. L. *Shapes: Statistical shape analysis*. (2013). at <<http://CRAN.R-project.org/>>
- 1002 1003 49.Adams, D. & Otarola-Castillo, E. Geomorph: An r package for the collection and analysis
1004 of geometric morphometric shape data. *Methods in Ecology and Evolution* **4**, 393–399 (2013).
- 1005 50.Wickham, H. *Ggplot2: Elegant graphics for data analysis*. (Springer New York, 2009).
1006 at <<http://had.co.nz/ggplot2/book>>